CHAPTER 6

SPECIAL STUDIES

Developing strategies to improve visibility requires an understanding of the relationship between the various aerosol species and atmospheric extinction. In this report and for applications where detailed physio-chemical aerosol characteristics are not known, the following equation is used to estimate extinction under the assumptions of external mixing, constant dry specific scattering, and sulfate interpreted as ammonium sulfate:

$$b_{ext} = (3)([SULFATE] + [NITRATE])\, f(RH) + (4)[OMC]\, f_{org}(RH) + (1)[SOIL] + (0.6)[CM] + (10)LAC \quad (6.1)$$

where b_{ext} is the reconstructed extinction coefficient. The ratio between dry and wet scattering as a function of relative humidity (RH) is referred to as the relative humidity scattering enhancement factor, f(RH). f(RH) and f_{org}(RH) refer to the enhancement factors for sulfates and nitrates, and organics, respectively. [SULFATE] is the ammonium sulfate concentration, while [NITRATE], [OMC], [SOIL], [CM], and [LAC] are the concentrations of ammonium nitrate, organic carbon, soil, coarse mass, and light-absorbing carbon, respectively. Light-absorbing carbon [LAC] and elemental carbon [EC] are used interchangeably throughout the chapter. Coarse mass is assumed to be primarily crustal in nature. The coefficient numbers refer to the assumed dry specific scattering of the respective species in m^2/g. The choice of these specific scattering coefficients are discussed in Malm et al. [1994] and are basically best estimates based on an extensive literature review and reported in Trijonis and Pitchford [1987] and Trijonis et al. [1990].

Average f(RH) values for each sampling period are calculated using Tang's [1996] ammonium sulfate D/D_o curves smoothed between the crystallization and deliquescent points. The f(RH) values are calculated for each hour and then averaged up to the sampling period length assuming a lognormal sulfate species mass size distribution, with an assumed geometric mass mean diameter and geometric standard deviation. The f(RH) associated with nitrates was assumed to be the same as for sulfates, while f_{org}(RH) for organics is set equal to one.

Understanding the inherent uncertainties in linking aerosol species concentrations to extinction using Equation (6.1) is essential if one is going to track progress in extinction change (change in visibility) as a function of changing emissions and resulting aerosol concentrations. Some key concerns are:

- How important are the mixing characteristics of aerosol species? Equation (6.1) assumes externally mixed particles, while it has been well documented that some species are internally mixed.
- What is the significance of scattering properties of sulfates as a function of ammoniation? This includes the water absorption properties of sulfates as a function of ammoniation.
- How important is the variability of ambient particle size to estimates of dry mass scattering efficiencies?
- What are the hygroscopic characteristics of organics?
- Is the assumption that coarse mass is primarily crustal valid and if not does its mass scattering efficiency vary significantly?
- Do carbon aerosols, other than elemental carbon, absorb light and if so what are the associated absorption efficiencies?
- Are the assumptions inherent to estimating extinction from aerosol species regionally dependent? Is the east different from the inner-mountain west or the northwest or the southwest?

6.1 GREAT SMOKY MOUNTAINS STUDY

Over the past five years, a number of special studies have been designed to answer some of these questions. During the summer months, the national parks in the eastern United States and the eastern United States as a whole experience some of the worst visibility conditions in the nation. Typically, high relative humidity conditions combine with high aerosol loading to reduce visibility to as low as 5-10 km, which corresponds to extinction levels of 0.4-0.8 1/km (or 400-800 1/Mm) To study these conditions, the Southeastern Aerosol and Visibility Study (SEAVS) was conducted from July 15, 1995, through August 25, 1995, in Great Smoky Mountains National Park. The study was a collaborative effort between several universities, consulting firms, the Electric Power Research Institute (EPRI), and the National Park Service (NPS). The overall objectives of this research were to better understand the physical, chemical, and overall optical characteristics of the ambient aerosol under the humid conditions observed in the southeastern United States during the summer months, and the relationships between these characteristics and visibility issues.

This discussion will focus on theoretically exploring the scattering properties of ambient aerosols as a function of mixing assumptions, sulfate ammoniation, aerosol size characteristics, and hygroscopic properties. Initiatory experiments on the relationship between measured water uptake and aerosol composition have been carried out by Zhang et al. [1993] and McMurry et al. [1996]. They used tandem differential mobility analyzers (TDMA) in conjunction with mass size sampling systems to measure growth as a function of size, composition, and relative humidity (RH). Saxena et al. [1995] and Pitchford and McMurry [1994] used their data to theoretically explore how water might be apportioned between the inorganic and organic aerosol fractions and as a function of mixing characteristics. Saxena et al. [1995] concluded that aerosols behaved differently at Grand Canyon, Arizona, than at the more urban site of Claremont, California. At Grand Canyon, they concluded that organics add to water absorption by inorganics. In the RH range of 80-88%, they assert that about 25-40% of water uptake is attributable to organics. On the other hand, Pitchford and McMurry [1994], using the same data set, demonstrated that all the water could be accounted for by assuming that just sulfate and nitrates, were hygroscopic. At Claremont,

Saxena et al. [1995] show that in the RH range of 80-93% the net effect of organics is to diminish water absorption by inorganics by 25-35%.

A number of authors have discussed the limitations of trying to apportion scattering to specific species, commonly referred to as scattering budgets [McMurry et al., 1996; White, 1986; Malm and Kreidenweis, 1997]. However, the goal of the calculations presented in this report is not to apportion scattering to any particular species, but to examine the ability of various models to predict scattering by fine particles (less than 2.5 μm) as a function of relative humidity and to draw from these calculations a better understanding of the hygroscopic characteristics of various aerosol types.

Experiments were designed such that observables could be estimated or modeled in a number of different ways. Measured ambient scattering at ambient relative humidities will be compared to ambient reconstructed scattering, and the ability of aerosol scattering models to predict the ratio of wet-to-dry scattering as a function of humidity will be explored. Modeling ambient scattering and the wet-to-dry scattering ratio will serve to both explore the validity of aerosol growth and mixing models and associated assumptions, and provide an estimate of the hygroscopicity of aerosol species other than sulfates and nitrates.

6.1.1 Experimental Methods

6.1.1.1 Humidograph

The hygroscopic properties are examined using a humidograph with the ability to measure scattering as a function of humidity over ranges of about 15-95%. Day et al. [1997] describe the instrument design in some detail and therefore its operation will only be summarized here.

Air is drawn through a temperature controlled humidity conditioner and passed into a Radiance Research M903 integrating nephelometer. The humidity conditioner consists of Perma Pure Nafion dryers, while temperature is controlled by placing the dryers in a constant temperature water bath. Because temperature change in the sampling plumbing can cause unwanted and unknown RH changes, temperatures are monitored throughout the system.

6.1.1.2 Integrating Nephelometers

The details of ambient nephelometer measurements were covered in Malm et al. [1994] and Day et al. [1997] and as before will only be briefly reviewed here. Five Optec NGN-2 integrating nephelometers, in various configurations, were operated during SEAVS. One of the five Optec nephelometers utilized the open-air configuration and was operated using standard IMPROVE protocols [Air Resource Specialists, 1994]. The other four Optec nephelometers were operated at reduced flow rates (113 l/min) and were fitted with an inlet, to which a Bendix-240 cyclone, with a 2.5 μm cutpoint could be attached. Two of these nephelometers were operated with an inlet and a cyclone. The other two nephelometers were operated with the inlet but without the cyclone. The four nephelometers that were operated with the inlet and at a reduced flow rate were much more susceptible to heating the sample aerosol in the optical chamber than was the open-air nephelometer. These nephelometers were therefore configured

with a water jacket mounted on the back wall of the scattering chamber. This water jacket surrounded the light source where most of the heat in the system was generated. Water was circulated through the water jacket inside the nephelometer, then through a heat exchanger outside the nephelometer that was kept at ambient temperature by a large fan. Thermistors were placed inside the inlet, where sample air was assumed to be at ambient temperature, and at the sample exit, where sample air should be hottest if heating of the aerosol had occurred. Monitoring the difference in sample temperature between the inlet and the outlet of each nephelometer allowed determination of whether heating of the sample had occurred and if there was a subsequent change in sample RH. Generally, the degree to which the sample was heated was less than 0.5°C. The accuracy of the nephelometer measurements and degree of heating are discussed in some detail by Day et al. [1997].

6.1.1.3 Relative Humidity Sensors

Three Rotronics mp 100f combination relative humidity/temperature sensors were housed in PVC holders and aspirated by a fan. The reported accuracy of the relative humidity sensor is ±2% [Rotronic Instrument Corp., 1998]. The flow rate through the holder was approximately 120 l/min. The sensors were approximately 6 ft above ground level, 6 ft from each other, and mounted near the inlets of the nephelometers.

6.1.1.4 Particulate Samplers

IMPROVE particle samplers were used throughout the study. A detailed description of validation and quality assurance procedures is available in Malm et al. [1994], Sisler et al. [1993], and Eldred et al. [1988]. In the most general sense, validation is a matter of comparing chemically related species that have been measured in different channels. Details of standard methods for apportionment of measured mass to the various aerosol species are described in some detail in Malm et al. [1994], however, in this study sulfate ammoniation was explicitly addressed.

Most fine sulfates are the result of oxidation of SO_2 gas to sulfate particles. In humid atmospheres, the oxidation of SO_2 occurs primarily in the aqueous phase where sulfuric acid is formed within water droplets. If there is inadequate ammonia in the atmosphere to fully neutralize the sulfuric acid, as is sometimes the case, then the resulting aerosols are acidic. Under these circumstances solutions of continuously varying acidity are formed. The extremes of this continuum are ammonium sulfate (neutral) and sulfuric acid.

Therefore, the ammoniated sulfate mass is estimated from independent measurements of SO_4 and NH_4 ions using:

$$[SO_{4,mass}] = (0.944)[NH_4^+] + (1.02)[SO_4^{2-}] \qquad (6.2)$$

where $[SO_{4,mass}]$ is the mass of the ammoniated sulfate compound.

6.1.2 Estimating Particle Scattering

Measurements of scattering used in the following analysis were restricted to particles less than 2.5 μm. A particle in the atmosphere can be a mix (internal mixture) of various aerosol species or in some cases its compositional structure may be restricted to one species (external mixture) such as $(NH_4)_2SO_4$. Whether the particles are internally or externally mixed they scatter or absorb a specific fraction of radiant energy that can be theoretically calculated by invoking a number of assumptions concerning the chemical and physical properties of the assumed structure of the aerosol. Following the suggestion of White [1986] the scattering/extinction per unit mass will be referred to as specific scattering/extinction as in specific gravity.

Comparisons between measured and theoretically reconstructed scattering will be carried out using four models. First, an externally mixed aerosol model with constant dry specific scattering, one sulfate species and associated growth as a function of relative humidity for that sulfate species was assumed. Second, an external model with constant specific scattering was assumed but the mass associated with sulfate ammoniation was calculated using Equation (6.2) and the functional dependence of scattering on RH is based on measured pure-component sulfate hygroscopic growth curves interpolated to the measured degree of neutralization. Third, the same model is assumed but sulfate specific scattering is estimated from measured sulfur mass size distributions. Finally, an internally mixed aerosol model is used that is based on measured sulfate ammoniation and size distributions with an assumed mass size distribution for other aerosol species.

To make reference to the various models the following modifiers to variables will be used: *E* and *M* refer to externally and internally mixed models, respectively, e_c and e_s to specific scattering assuming a constant and size dependent value, S_c and S_a refer to a fixed sulfate species such as ammonium bisulfate, and ammoniated sulfate, respectively, while *B*, *C*, and *D* refer to the best estimate, crystallization, and deliquescent growth curves. For instance, $b_{scat}\_E\_e_s\_S_a\_B$ refers to modeled scattering assuming an external model (*E*), size dependent specific scattering coefficient (e_s), ammoniated sulfate (S_a), and best estimate hygroscopic growth curve (*B*). b_{scat} refers to modeled scattering, while $<b_{scat}>$ is measured scattering.

6.1.2.1 Aerosol Growth as a Function of Relative Humidity

Tang [1996] published data on growth curves, D/D_o, as a function of increasing and decreasing relative humidity for $(NH_4)_2SO_4$, NH_4HSO_4, and H_2SO_4. For increasing or decreasing RH, $(NH_4)_2SO_4$ and NH_4HSO_4 exhibit a hysteresis in the D/D_o vs RH relationship, with sharp discontinuities at the deliquescence (relative humidity at which the crystal abruptly absorbs water) and crystallization (relative humidity at which particle abruptly loses water and recrystalizes) humidities. However, because vertical atmospheric mixing during summer months in the eastern United States should almost always bring the aerosol into an RH environment that is in excess of 80% one can make the argument that the sulfate aerosol will always be on the crystallization (upper) branch of the aerosol growth curve. Furthermore, because mixtures of ammoniated sulfate compounds with other species have been shown to be hygroscopic below the deliquescent values [Sloane, 1984, 1986; Stelson and Seinfeld, 1982], and

because the growth factor and light-scattering efficiency for ambient aerosols has previously been observed to be rather smooth [Sloane, 1983, 1984, 1986; Wexler and Seinfeld, 1991; Waggoner et al., 1981] it is not known whether the upper or lower limb of the hysteresis curve applies for a particular aerosol sample. Therefore, as our "best estimate" for the sulfate species growth, the curves were smoothed between the deliquescence and crystallization points.

At the Great Smoky Mountains National Park monitoring site, the neutralization of the sulfate aerosols varied from sampling period to sampling period. As an estimate of sulfate compound hygroscopicity for aerosols whose molar ratios of ammonium to sulfate were somewhere between 0 and 2, a linear interpolation between growth curves was carried out based on NH_4 to SO_4 ratios.

When species with different hygroscopic characteristics, such as organics and sulfates, are internally mixed, a method for adjusting the aerosol hygroscopicity in response to changes in chemical composition is needed. Malm and Kreidenweis [1997] have demonstrated the application of the Zdanovskii-Stokes-Robinson (ZSR) model, which accounts for solute-solvent interactions but neglects solute-solute interactions. The use of the ZSR model for determination of the water content has been utilized by Saxena and Peterson [1981]. They examined the applicability of the ZSR assumptions to mixtures of inorganics, while Meng et al. [1995] applied it to mixtures of organics and inorganics. In the present case, the ZSR model assumptions were used to derive an equation for the hygroscopic growth of internally mixed particles when the growth characteristics of the externally mixed species are either known or can be approximated. Applying the ZSR model assumptions to the case of two solute species yields:

$$\left(\frac{D}{D_o}\right)^3 = \frac{\rho_{dry}}{\rho_{wet}}\left[z_1\frac{\rho_{wet1}}{\rho_{dry1}}\left(\frac{D_1}{D_{o,1}}\right)^3 + z_2\frac{\rho_{wet2}}{\rho_{dry2}}\left(\frac{D_2}{D_{o,2}}\right)^3\right] \tag{6.3}$$

D and D_o are the dry and wet particle diameter, ρ_{dry} and ρ_{wet} are the dry and wet densities and the subscript 1 and 2 refer to species one and two. The coefficients z_1 and z_2 are the mass fractions of each species. It should be noted that models that treat water uptake for nonideal, multicomponent solutions using theoretical and semi-theoretical thermodynamic relationships have been developed and have been applied to both visibility and climate forcing problems [Saxena and Peterson, 1981; Pilinis et al., 1995; Saxena et al., 1986, 1993]. The correct treatment of the hygroscopicity of species in multicomponent mixtures—especially organic species—remains problematic, not only because of the lack of suitable mixture thermodynamic data, but also because of the lack of information about other critical mixture properties.

6.1.2.2 Estimation of Size Dependent Specific Scattering

The analysis of DRUM measured sulfur size distributions is confined to the five stages that collect particles with a diameter below 2.5 μm. The size-resolution afforded by the five size cuts is quite limiting when estimating scattering efficiencies using Mie theory because particles collected on each stage cover quite a large variation in size. For instance, particles between 0.07 and 0.24 μm are collected on stage one. Therefore, the mass size distributions are usually "inverted" to yield a smoothed estimate of *dC/dlog(D)* [John et al., 1990]. DRUM measurements are inverted using the Twomey [1975] scheme, which is a nonlinear iterative algorithm that

accounts for the sampling efficiency as a function of particle size for each stage. The output of the inversion is 72 data pairs of *dC/dlog(D)* and *D*, where *C* is the concentration of sulfur and *D* is the aerodynamic diameter. Geometric mass mean diameter and geometric standard deviation are calculated for each of these sulfur size distributions using Stokes diameters.

Using Mie theory specific scattering was calculated from *dC/dlog(D)* distributions three different ways. First, the dry sulfate specific scattering (e_d) was calculated by estimating the dry scattering coefficient ($b_{scat,d}$), assuming water was not mixed with the particle (RH=0.0%), and dividing that scattering by dry ammoniated sulfate mass concentration. Because the "wet" size is measured by the DRUM sampler the dry size was calculated using the sampling period average (D/D_o) corresponding to the ambient RH. (D/D_o) was estimated as discussed above for each hour and then averaged up to twelve hours. Second, a wet ammoniated sulfate specific scattering (e_w) was arrived at by calculating the scattering of the sulfate species plus water ($b_{scat,w}$) and dividing it by the mass of sulfate species plus water. Finally, the water enhanced efficiency (e_{wd}) was calculated by dividing the scattering of the wet ammoniated sulfate species by dry ammoniated sulfate mass. The water associated with the ammoniated sulfate species mass was calculated assuming volume conservation between sulfate and water. The index of refraction of the "wet" aerosol was arrived at by volume weighting the index of refraction for sulfate species and water.

For the internally mixed model, the calculations were carried out in much the same way, however, the growth was estimated using Equation (6.3). As before the water associated with the internally mixed aerosol mass was calculated assuming volume conservation and the index of refraction of the "wet" aerosol was arrived at by volume weighting the index of refraction for sulfate species, nitrates, organics, and water. The indices of refraction used in the calculations were 1.41, 1.47, 1.53, 1.55, 1.55, 1.53, and 1.33 for sulfuric acid, ammonium bisulfate and sulfate, ammonium nitrate, organics, soil, and water, respectively.

6.1.2.3 The Externally Mixed – Constant Dry Specific Scattering Model

The following equation is used to estimate scattering under the assumptions of external mixing, constant dry specific scattering, and sulfate interpreted as ammonium bisulfate or sulfate mass adjusted for the level of ammoniation:

$$b_{scat} = (3)([SULFATE] + [NITRATE])\, f(RH) + (4)[OMC]\, f_{org}(RH) + (1)[SOIL] \qquad (6.4)$$

b_{scat} is the reconstructed scattering coefficient. The ratio between dry and wet scattering as a function of RH is referred to as the relative humidity scattering enhancement factor, f(RH). f(RH) and f_{org}(RH) refer to the enhancement factors for sulfates, nitrates, and organics, respectively. [SULFATE] is the SO_4 ion mass concentration adjusted either to a constant sulfate species type, such as ammonium bisulfate, or for its level of ammoniation. [NITRATE], [OMC], and [SOIL] are the concentrations of ammonium nitrate, organic carbon, and soil. The coefficient numbers refer to the assumed dry specific scattering of the respective species in m^2/g. The choice of these specific scatterings are discussed in Malm et al. [1994] and are basically best estimates based on an extensive literature review and reported in Trijonis and Pitchford [1987] and Trijonis et al. [1990].

Average *f*(RH) values for each sampling period were calculated using Tang's sulfate D/D_o curves. The *f*(RH) values were calculated for each hour and then averaged up to the sampling period length assuming a lognormal sulfate species mass size distribution with a geometric mass mean diameter of 0.3 μm and a geometric standard deviation, σ_g, of 1.5 was assumed. Estimates of *f*(RH) were derived for the deliquescent and crystallization curves as well as for curves that were smoothed between the crystallization and deliquescent points. The *f*(RH) associated with nitrates was assumed to be the same as for sulfates, while f_{org}(RH) for organics was set equal to one.

6.1.2.4 The Externally Mixed–Sulfate Ammoniated–Variable Specific Scattering Model

The following equation was used to estimate scattering:

$$b_{scat} = e_{wd}([SULFATE] + [NITRATE]) + (4)[OMC] f_{org}(RH) + (1)[SOIL] \quad (6.5)$$

e_{wd} is the ammoniated size and relative humidity dependent scattering efficiency of the wetted sulfate aerosol and the variables in the brackets are the dry mass concentrations of the various species. It is assumed that the nitrate and sulfate size distributions are the same and that nitrates scatter with the same efficiency as sulfate. The other variables are the same as those defined above.

6.1.2.5 The Internally Mixed Variable Mass and Size Scattering Model

The equation used to reconstruct scattering when the sulfate size distribution is known and a size distribution for organics and nitrates is assumed by:

$$b_{scat} = e_{wdm}([SULFATE] + [NITRATE] + [OMC]) + (1)[SOIL] \quad (6.6)$$

where e_{wdm} is the size and relative humidity dependent specific scattering for a sulfate, nitrate, and organic aerosol that is uniformly mixed. It is assumed that soil is externally mixed.

6.1.3 Results

6.1.3.1 Summary of Aerosol Measurements

$PM_{2.5}$ Measurements. Table 6.1 contains statistical summaries of the aerosol fine mass ($PM_{2.5}$) concentrations along with the fraction that each aerosol species contributes to reconstructed fine mass. All sampling periods were twelve hours in length starting at 7:00 a.m. Figure 6.1 shows temporal plots of measured fine mass and the five major aerosol species. The lowest concentrations of fine mass occurred on Julian day (JD) 216 when values of 3-4 $\mu g/m^3$ were recorded. Conversely, on JD 230 measured fine mass was 88 $\mu g/m^3$. Three relatively high soil episodes were recorded on JD=206-207, JD=215-216, and JD=225-232. On JD=207 soil was about 40-50% of the fine mass. The contributions of elemental carbon (EC) and nitrate to fine mass were small during the entire study period.

Table 6.1 *Statistical summary of aerosol species concentrations and the fraction of reconstructed fine mass attributed to certain species. FM, reconstructed FM, [SO_4] ion, [SULFATE], [NH_4NO_3], [OMC], [EC], [SOIL], [CM], and [NH_4] are gravimetric fine mass, reconstructed fine mass, sulfate ion mass, sulfate plus ammonium mass, neutralized nitrate mass, organic carbon mass, elemental carbon mass, soil mass, coarse mass, and ammonium ion mass, respectively.*

Variable	Mean ($\mu g/m^3$)	Std. Dev.	Minimum ($\mu g/m^3$)	Maximum ($\mu g/m^3$)	Fraction	N
FM	25.13	17.55	0.00	87.94	1.38	80
Reconstructed FM	18.09	12.34	3.66	59.41	---	80
[SO_4] ion	9.55	9.02	1.09	42.71	---	80
[SULFATE]	11.42	10.32	1.17	48.23	0.63	80
[NH_4NO_3]	0.20	0.11	0.07	0.70	0.01	80
[OMC]	4.56	1.79	1.40	8.60	0.25	80
[EC]	0.44	0.25	0.00	1.17	0.02	80
[SOIL]	1.47	1.56	0.02	8.33	0.08	80
[CM]	6.16	5.85	0.00	24.69	---	80
[NH_4]	1.79	1.30	0.06	4.98	---	80
NH_4/SO_4 molar ratio	1.10	0.30	0.30	1.85	---	80

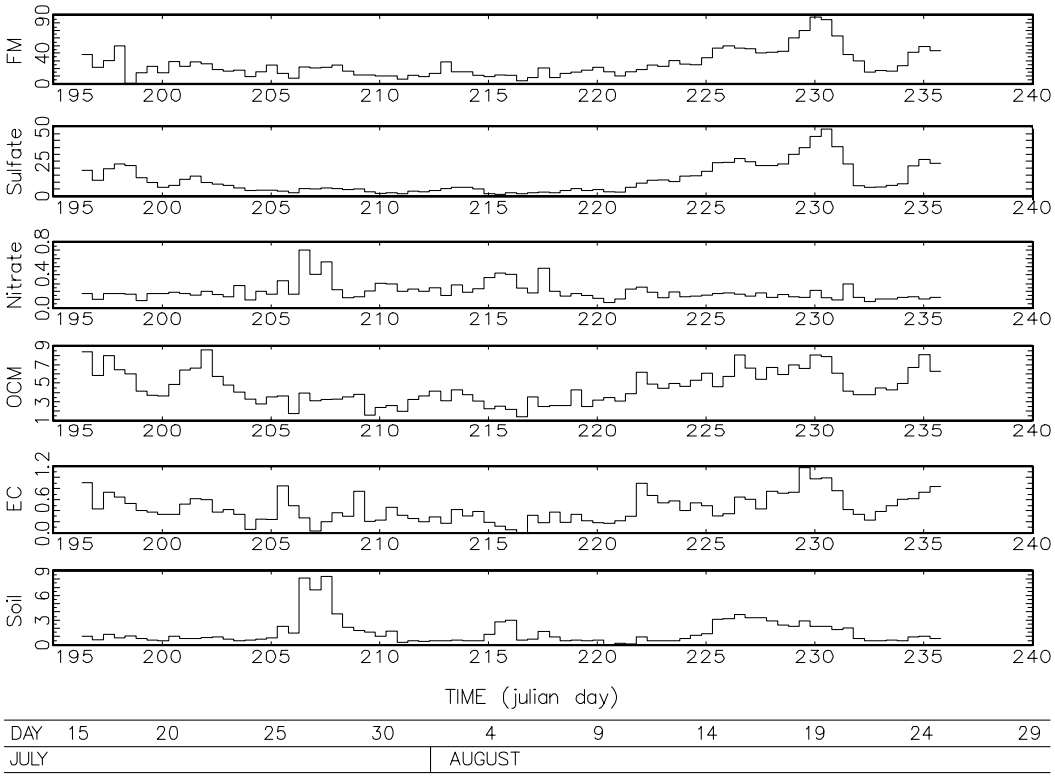

Figure 6.1 *Time lines of fine mass (FM), sulfate species mass (Sulfate), ammonium nitrate (Nitrate), organic mass (OCM), elemental carbon (EC), and soil (Soil). The time line is presented in Julian day, while concentrations are in $\mu g/m^3$.*

On the average, measured fine mass accounted for about 80% of the measured PM_{10} mass. Sulfates were the largest fraction of reconstructed fine mass at 63%. Organic carbon accounted for 25% of the fine mass, while soil contributed another 8%. Nitrates and EC were virtually tied for the lowest contribution to fine mass at 1% and 2%. It is worth noting that the mass fractions reported here are consistent with those found at other eastern monitoring sites [Sisler, 1996]. The average molar ratio of ammonium to sulfate ion was about 1, indicating that the sulfate ion was, on the average, about half neutralized.

Sulfur Mass Size Distributions. Figures 6.2 and 6.3 show two sulfur mass size distributions for two sampling periods. Figure 6.2 shows a mass size distribution for "larger sulfur particles", while Figure 6.3 is a more "typical distribution". Included on each graph are the Δ(sulfate mass)/Δ(log(*D*)) values derived directly from the DRUM sampler and from the results of the Twomey inversion calculation. The peak or maximum Δ(sulfur mass)/Δ(log(*D*)) curve for the more typical distribution occurred at about 0.45 μm, while for the "large" size distribution the maximum occurred at near 0.6 μm with most of the mass being above about 0.4 μm.

Table 6.2 is a statistical summary of the relative humidity, water mass associated with the sulfate species at ambient humidity, sulfate plus ammonium mass as measured with the IMPROVE and DRUM samplers, wet geometric mass mean diameter, and the geometric standard deviation. Various scattering parameters, which will be discussed in the next section, are also summarized.

The average ammoniated sulfate species concentrations are 14.95 and 14.02 $\mu g/m^3$ for the IMPROVE and DRUM samplers, respectively, which corresponds to a difference of 6.2%. The average geometric mass mean diameter at ambient RH is 0.36 μm with an average geometric standard deviation of 1.92.

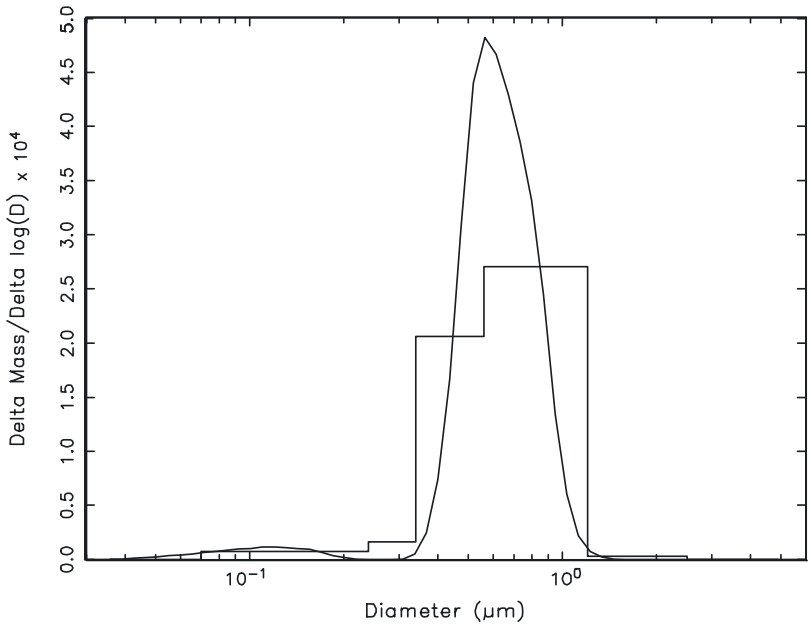

Figure 6.2 *An elemental sulfur mass size distribution at ambient RH for JD 229, which corresponds to a σ_g of 1.5 and a D_g equal to 0.60 μm. The smooth curve is the mass size distribution calculated using the Twomey [1975] inversion technique.*

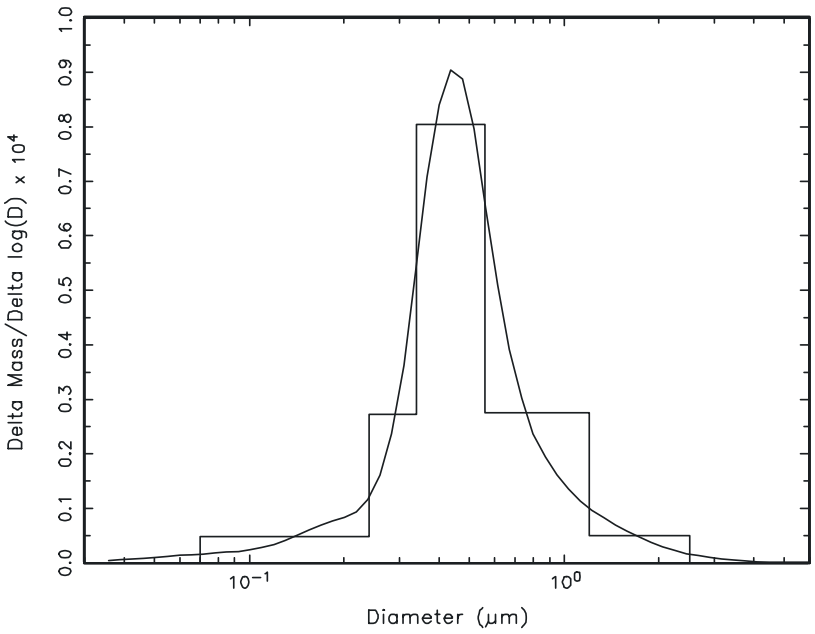

Figure 6.3 *A sulfur mass size distribution at ambient RH for JD 237, which corresponds to a σ_g of 1.8 and a D_g equal to 0.47 μm. The smooth curve is the mass size distribution calculated using the Twomey [1975] inversion technique.*

Table 6.2 *Statistical summary of DRUM data. WMASS is water mass associated with sulfate aerosol at ambient relative humidity, $SO_{4,mass}$ is sulfate plus ammonium mass, D_g and σ_g are the wet geometric mass mean diameter and standard deviation, respectively. e_d and e_w are the specific scattering of the dry and wet sulfate aerosol, while e_{wd} is wet scattering divided by the dry mass.*

Variable	Mean	Std. Dev.	Minimum	Maximum	N
RH (%)	74.99	8.94	51.66	92.24	45
WMASS ($\mu g/m^3$)	20.57	14.56	2.33	66.60	45
IMPROVE $SO_{4,mass}$ ($\mu g/m^3$)	14.95	11.37	2.09	48.23	45
DRUM $SO_{4,mass}$ ($\mu g/m^3$)	14.02	10.27	1.29	44.50	45
D_g (μm)	0.36	0.07	0.18	0.50	45
σ_g	1.92	0.27	1.47	2.37	45
e_d (m^2/g)	2.40	0.51	1.33	3.10	45
e_w (m^2/g)	3.58	0.61	1.76	4.60	45
e_{wd} (m^2/g)	9.64	3.25	3.04	19.12	45

Calculation of Sulfate Specific Scattering From Mass Size. The study's average dry specific scattering (e_d), wet specific scattering (e_w), and water enhanced specific scattering (e_{wd}) for sulfate are summarized in Table 6.2. e_d and e_w are 2.40 and 3.58 m^2/g, respectively. The mean dry specific scattering of 2.40 m^2/g is somewhat less than the 3.0 m^2/g used by a number of authors to estimate sulfate scattering [Trijonis et al., 1990]. The average enhanced specific scattering, e_{wd}, on the other hand, is 9.64 m^2/g at an average ambient relative humidity of 75%.

6.1.3.2 Comparison of Measured and Theoretical Predictions of Ambient Scattering

Results for the Externally Mixed Constant Specific Scattering Model. Because the average molar ratio of ammonium to sulfate ion was approximately one the ammonium bisulfate D/D_o curve was used to calculate the f(RH) function. [SULFATE] in Equation (6.4) was interpreted as ammonium bisulfate. Results of these calculations are summarized in Table 6.3 and shown in Figure 6.4, where measured and reconstructed scattering are scattered against each other. Also plotted in Figure 6.4 is the 1:1 line. The average sulfate scattering is 0.129 1/km, which in turn yields an average reconstructed scattering ($b_{scat}\_E\_e_c\_S_c\_f$(RH)), of 0.152 1/km, which is about 18% less than measured average scattering.

Table 6.3 *Statistical summary of measured scattering (<b_{scat}>), reconstructions of b_{scat} assuming different mixing rules and specific scattering and the scattering associated with each aerosol species. Except for f(RH), which is unitless, all units are in 1/km. The parenthetical values in the mean column are the fractional contribution of the respective species to the "best estimate" of reconstructed scattering. Variable descriptors are found at the bottom of the table.*

Variable	Mean	Std. Dev.	Minimum	Maximum	N
$< b_{scat}>$	0.185	0.133	0.045	0.611	45
$b_{scat}\_E\_e_c\_S_c\_f(RH)$	0.152	0.098	0.033	0.454	45
$b_{scat}\_E\_e_c\_S_a\_f(RH)$	0.164	0.118	0.037	0.537	45
$b_{scat}\_E\_e_s\_S_a\_B$	0.168	0.130	0.028	0.596	45
$b_{scat}\_E\_e_s\_S_a\_C$	0.168	0.129	0.028	0.596	45
$b_{scat}\_E\_e_s\_S_a\_D$	0.164	0.132	0.028	0.596	45
$b_{scat}\_M\_e_s\_S_a\_B$	0.182	0.134	0.033	0.626	45
RH (<95%)	74.99	8.94	51.66	92.24	45
f(RH)	3.29	1.07	1.44	6.57	45
$SO_4\_e_c\_S_c\_f(RH)$	0.129	0.093	0.020	0.420	45
$SO_4\_e_c\_S_a\_f(RH)$	0.140	0.113	0.024	0.502	45
$SO_4\_e_s\_S_a\_B$	0.143(0.85)	0.125	0.015	0.562	45
$SO_4\_e_s\_S_a\_C$	0.143	0.125	0.015	0.562	45
$SO_4\_e_s\_S_a\_D$	0.139	0.128	0.015	0.562	45
OC	0.021(0.13)	0.007	0.010	0.034	45
NO_3 *f(RH)*	0.002 (0.01)	0.001	0.001	0.004	45
Soil	0.002 (0.01)	0.002	0.000	0.008	45

E=external mixture
M=internal mixture
e_c=constant specific scattering
e_s=size dependent specific scattering
S_c=fixed sulfate species (NH_4HSO_4)
S_a=ammoniated sulfate species
B=best estimate sulfate growth curves
C=crystallization sulfate growth curves
D=deliquescent sulfate growth curves

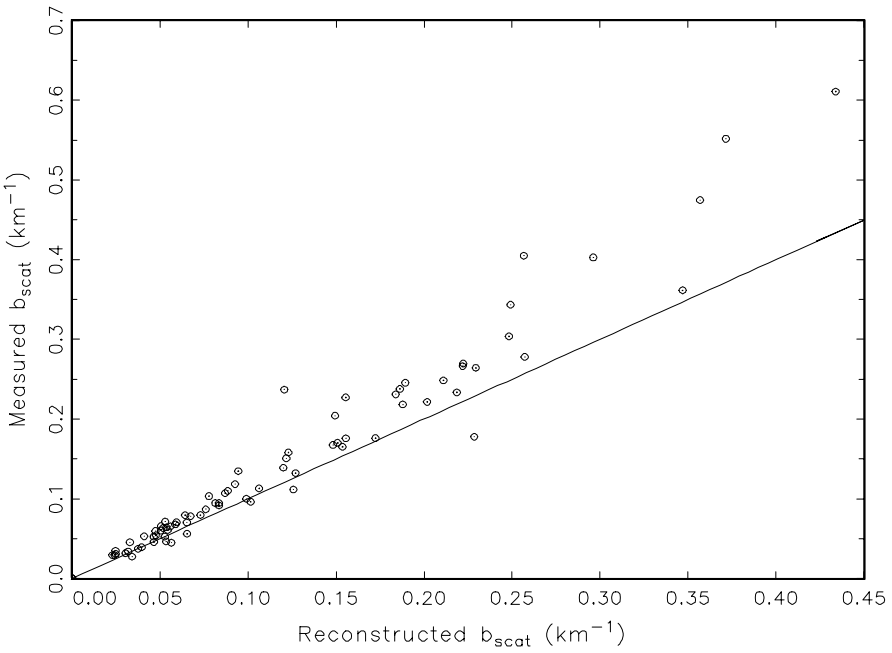

Figure 6.4. *An example of a measured f(RH) curve on sampling period corresponding to JD 205.29. The curve through the data points is a best fit using an equation with a functional form containing RH/(1-RH).*

An ordinary least square (OLS) regression yielded a very high R^2 of 0.95, however, the OLS regression line is about 1.31, implying measured scattering is about 30% greater than reconstructed. Similar discrepancies between reconstructed and measured scattering were noted previously [Gebhart and Malm, 1990] using data gathered at Shenandoah National Park. For the most part the use of Equation (6.4) and [SULFATE] as ammonium bisulfate or ammonium sulfate to reconstruct scattering works well for most western IMPROVE sites [Malm et al., 1996]. The inability to use Equation (6.4) and the associated assumptions to reconstruct scattering at nonurban eastern sites was part of the motivation for carrying out SEAVS.

The calculations were repeated using Equation (6.4) but with [SULFATE] explicitly adjusted for the ammonium ion concentration and the *f*(RH) function for the ammoniated sulfate aerosol species was calculated on a sampling-period-by-sampling-period basis using Tang's sulfate D/D_o curves that were smoothed between the crystallization and deliquescent points and interpolated between $(NH_4)_2SO_4$, NH_4HSO_4, and H_2SO_4, as described previously. $SO_4\_e_c\_S_a\_f$(RH) is 0.140 1/km, which in turns yields an average reconstructed scattering ($b_{scat}\_E\_e_c\_S_a\_f$(RH)), of 0.164 1/km, compared with 0.152 1/km for the case that did not use actual sulfate compound mass concentrations nor an estimation of the amount of water associated with each type of sulfate species. This is still about 11% lower than measured scattering. The R^2 of an OLS regression between reconstructed and measured scattering is again high at over 0.95 and the regression coefficient is 1.12, suggesting the measured scattering is about 12% greater than reconstructed.

Results for the Externally Mixed Model with Sulfate Specific Scattering Estimated From Mass Size Distributions. The same strategy described previously, for estimating D/D_o was used. However, to develop the range of possible ammoniated sulfate and associated water scattering allied with the crystallization, deliquescent, and best estimate branches of the growth curves, each was used in the reconstructed scattering calculation and the results are presented in Table

6.3 under $SO_4\_e_s\_S_a\_C$, $SO_4\_e_s\_S_a\_D$, and $SO_4\_e_s\_S_a\_B$, respectively. There are only small differences between the three estimations. The crystallization $SO_4\_e_s\_S_a\_C$ is almost the same as the best estimate $SO_4\_e_s\_S_a\_B$, while the deliquescent $SO_4\_e_s\_S_a\_D$ is about 3% less than the best estimate. Because other species also contribute to scattering, the net effect of the three different assumptions on total $PM_{2.5}$ scattering is even less. Reconstructed scattering varies between 0.168 1/km and 0.164 1/km. Furthermore, reconstructed scattering using this model (sulfate scattering efficiencies estimated from mass size distributions) is nearly the same as the constant dry specific scattering model but with sulfate ammoniation accounted for. Apparently, the biggest effect in achieving a close match between reconstructed and measured scattering is the adjustment for sulfate ammoniation and associated growth as a function of relative humidity.

Results of the calculation are further highlighted in Figure 6.5, where the range of scattering coefficients associated with using the crystallization, best estimate, and deliquescent branches of the growth curve is shown. Also shown in the scatter plot is the 1:1 line. A visual examination of the scatter plot shows that reconstructed and measured scattering compare quite favorably. An OLS regression between measured and reconstructed scattering using the "best estimate" growth curves yields an R^2 of 0.98, a slope of 1.00, and an offset of 0.014 1/km. The parenthetical values in Table 6.3 are the study-averaged fractional contribution of each species to fine specific scattering using the "best estimate" growth model. Sulfates, organics, nitrates, and soil contribute 85%, 13%, 1%, and 1%, respectively.

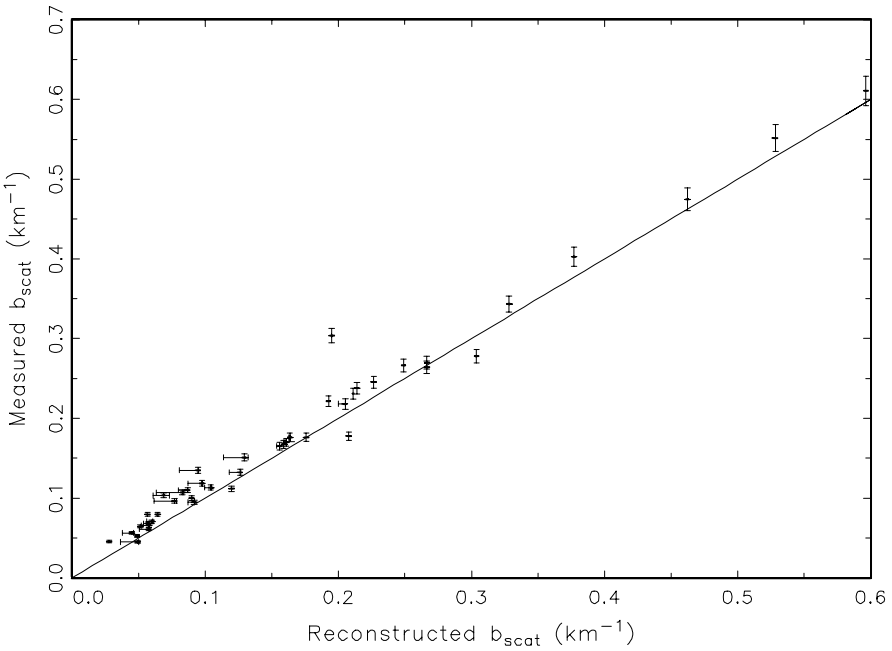

Figure 6.5 *A scatter plot of reconstructed and measured $PM_{2.5}$ scattering assuming external mixing but with measured sulfur size distributions. The range of reconstructed scattering was arrived at by assuming three different forms of Tang's D/D_o curves for $(NH_4)_2SO_4$, NH_4HSO_4, and H_2SO_4. The highest reconstruction is arrived at by using the crystallization branches, the middle value from a best estimate growth between the crystallization and deliquescence branches, while the lowest reconstruction was calculated using the deliquescent arm of the growth curves. Units are in 1/km.*

As an example of the temporal variability, Figure 6.6 shows the time lines of measured, ammoniated sulfate species, nitrate, organics, and soil scattering coefficients for the "best estimate" growth model. The units in Figure 6.6 are 1/km. Sulfate scattering varies from about 0.05 1/km to a high of over 0.6 1/km: over an order of magnitude change. Nitrate scattering varies around 0.002 1/km, while organics vary from about 0.004 to 0.04 1/km, also an order of magnitude change. However, the organic scattering coefficient is about an order of magnitude lower than that for sulfate. There is one soil episode occurring on JD 206-208, where the soil scattering is almost 0.01 1/km as compared to the more typical values of 0.002-0.003 1/km. It should be pointed out, however, that the episode soil scattering coefficient at 0.01 1/km is still about five times less than the lowest sulfate scattering coefficient.

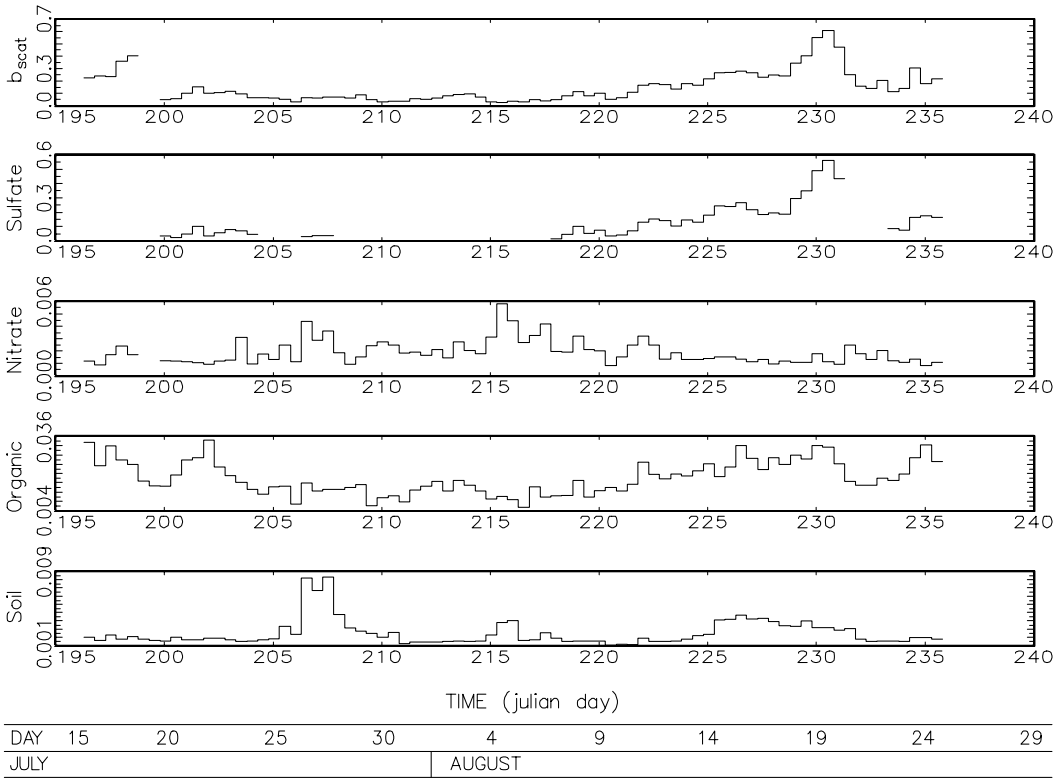

Figure 6.6 *Time lines showing measured <b_{scat}> (b_{scat}), sulfate species scattering (Sulfate), ammonium nitrate scattering (Nitrate), organic specific scattering (Organic), and soil scattering (Soil). The best estimate D/D_o growth curve and measured sulfur mass size distributions were used. Units on scattering are in 1/km, while time is presented as Julian day.*

Results for the Internally Mixed Model with Measured Sulfur Mass Size Distribution. For the internally mixed model, it was assumed that sulfates, nitrates, and organics were uniformly mixed, all with the same size distribution as sulfur. The growth of the mixed particle was calculated using Equation (6.4) for a three species mix and with D/D_o set equal to 1 for organics (that is, organics were considered nonhygroscopic), while nitrates were assumed to have the same hygroscopicity as sulfates. D/D_o for sulfate species was calculated using the "best estimate" growth curve as described above.

Results of the calculation are summarized in Table 6.3 as $b_{scat}\_M\_e_s\_S_a\_B$, while Figure 6.7 shows the internally and externally mixed model results plotted against measured scattering. The range of results for the internal and external model calculations is represented by the horizontal bars with the largest reconstructed scattering generally corresponding to the internal model and the lowest scattering with the external calculation. In most cases, the difference between the internal and external case is small, as expected. The average difference between the two calculations is only about 8%, with the internally mixed model yielding the higher reconstructed scattering estimates and in closer agreement with measurement.

An OLS regression between reconstructed scattering using the internally mixed model and measured scattering resulted in an R^2 of 0.97 with a slope of 0.97±0.025.

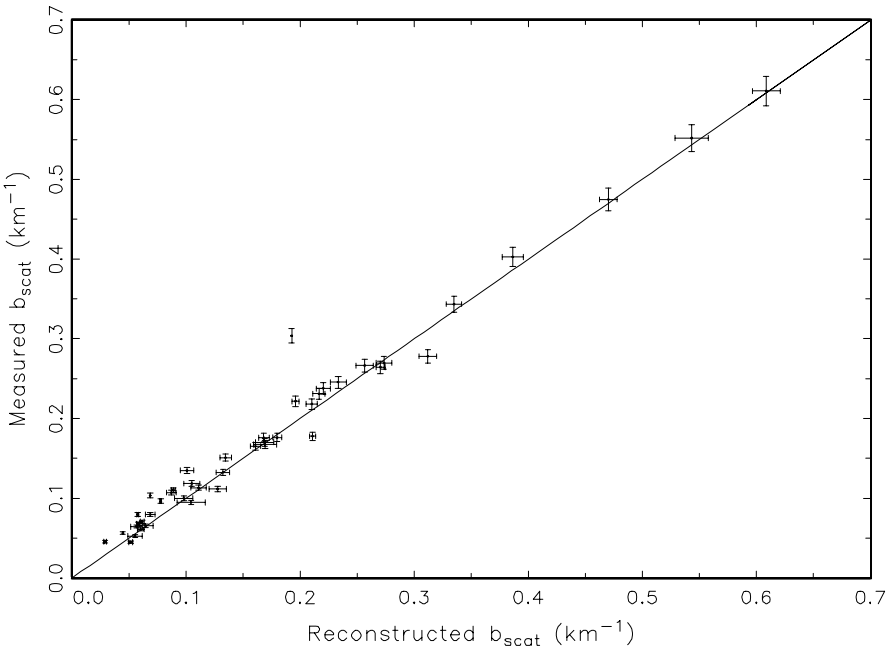

Figure 6.7 *Scatter plot of reconstructed and measured scattering along with the 1:1 line. The upper and lower bound of reconstructed scattering correspond to assuming an internally and externally mixed aerosol.*

6.1.3.3 Comparison of Measured and Theoretical Estimations of $b_{scat}(RH)/b_{scat,dry}$

Comparisons between measured and modeled calculations of $b_{scat}(RH)/b_{scat,dry}$ will be carried out using the latter three modeling approaches described previously. While most measurements were made from JD 196 to JD 235, the humidograph was only successfully operated from JD 203 to 225 and on JD 230, and the mass size measurements are available for most time periods between JD 199 and 207 and between JD 216 and 235. Therefore, out of 80 sampling periods where $b_{scat}(RH)/b_{scat,dry}$ model calculations could be done, there are only 24 overlapping time periods where all three model calculations can be compared. However, any single model comparison to $b_{scat}(RH)/b_{scat,dry}$ measurements can have more data points. For instance, the

comparison between measurements and the external model calculation, which does not rely on mass size distribution measurements, has 70 common sampling periods.

Figure 6.8 shows a comparison between measured and modeled $b_{scat}(RH)/b_{scat,dry}$ for JD 204.29. The three lines correspond to the model calculations, while the measured data points are represented by the uncertainty bars where uncertainty in the $b_{scat}(RH)/b_{scat,dry}$ ratio and relative humidity are shown. The solid line corresponds to the external-constant specific scattering model, $b_{scat}\_E\_e_c\_S_a\_f(RH)$, but with sulfate ammoniation and water uptake accounted for, the short dashed line is the external model with sulfate efficiency calculated from sulfur mass size distributions, $b_{scat}\_E\_e_s\_S_a\_B$, and the long dashed line corresponds to the internally mixed model, $b_{scat}\_M\_e_s\_S_a\_B$. In most cases, the external and mixed models agreed quite well with each other and with the measurements. However, there were a number of cases where all models agreed well with each other but the modeled $b_{scat}(RH)/b_{scat,dry}$ was well above measured values. One representative case is shown for JD 202.79 in Figure 6.9. In most cases, when modeled $b_{scat}(RH)/b_{scat,dry}$ was greater than the measured ratio, the organic fraction of fine mass was at its highest values. For instance, JD 202.79 corresponds to the sampling period with the highest organic concentration.

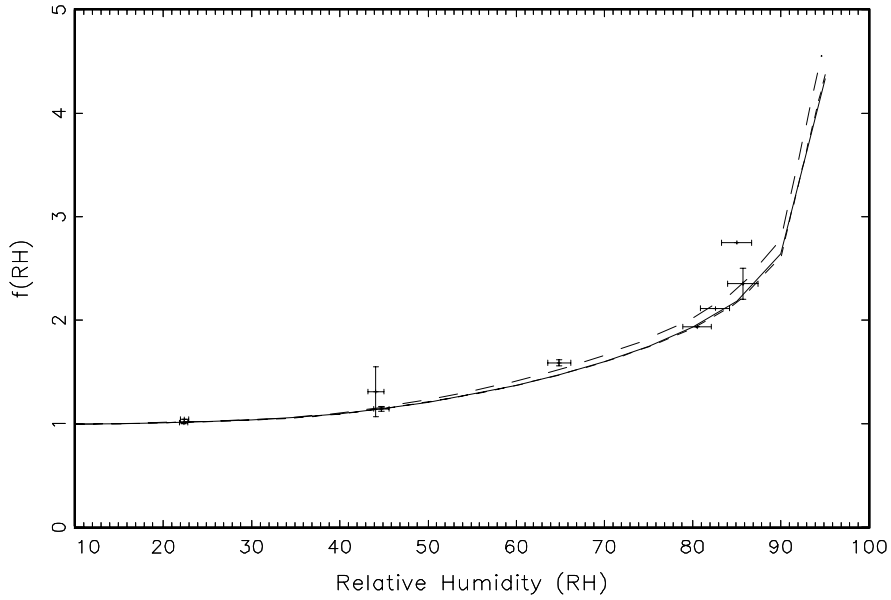

Figure 6.8 *f(RH), $b_{scat}(RH)/b_{scat,dry}$, is plotted as a function of relative humidity. The uncertainty bars represent the uncertainties in measured RH and f(RH), while the three lines correspond to the three model calculations. The solid line, small and large dashed lines correspond to external-constant specific scattering, external-variable specific scattering, and mixed model, respectively. Julian Day = 204.29.*

There are a few time periods where the mixed model $b_{scat}(RH)/b_{scat,dry}$ ratio was substantially lower than the ratios predicted by the external models. One example is shown in Figure 6.10 where the internally mixed and external model calculations bound the measured ratios. On JD 217 the internally mixed model ratios were lower than measured or external model predictions. The discrepancy between internally mixed and external model calculations occurred on the lowest sulfur concentration time periods. For those time periods, the mixed model predicts less of an increase in scattering as a function of relative humidity than do the external models.

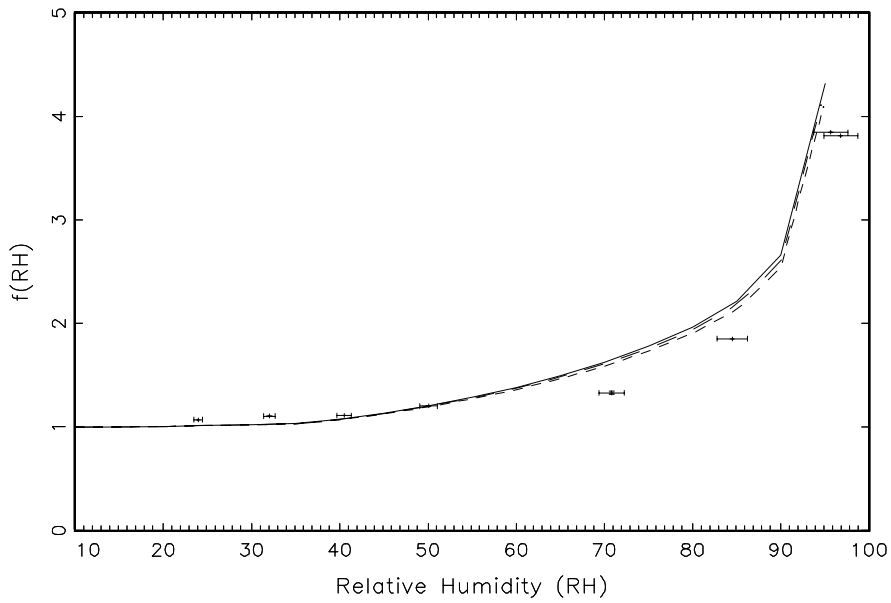

Figure 6.9 *f(RH), $b_{scat}(RH)/b_{scat,dry}$, is plotted as a function of relative humidity. The uncertainty bars represent the uncertainties in measured RH and f(RH), while the three lines correspond to the three model calculations. The solid line, small and large dashed lines correspond to external-constant specific scattering, external-variable specific scattering, and mixed model, respectively. Julian day = 202.79.*

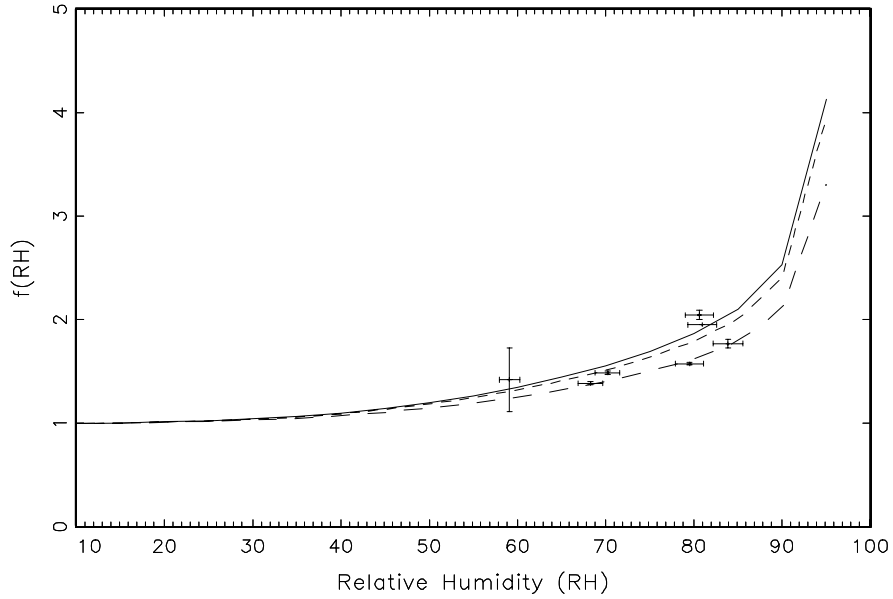

Figure 6.10 *f(RH), $b_{scat}(RH)/b_{scat,dry}$, is plotted as a function of relative humidity. The uncertainty bars represent the uncertainties in measured RH and f(RH), while the three lines correspond to the three model calculations. The solid line, small and large dashed lines correspond to external-constant specific scattering, external-variable specific scattering, and mixed model, respectively. Julian day = 206.79.*

Comparisons between measured and calculated $b_{scat}(RH)/b_{scat,dry}$ for the whole data set are shown in Figure 6.11 for the $b_{scat}\_E\_e_s\_S_a\_B$ model, while comparisons, using ordinary least square regressions, between measured and estimated ratios for all models are summarized in Table 6.4. Figure 6.11 shows that in general there is good agreement between measured and modeled $b_{scat}(RH)/b_{scat,dry}$ ratios. There are about eight data points where modeled ratios are significantly greater than measured values and at higher RH values model calculations appear to be slightly greater than measured ratios. The R^2 for regressions between measured and model calculations range from a high of 0.92 for the $b_{scat}\_E\_e_c\_S_a\_f(RH)$ to a low of 0.71 for the $b_{scat}\_M\_e_s\_S_a\_B$ model. All models yield $b_{scat}(RH)/b_{scat,dry}$ ratios that are about 20% greater than measured values. In all models, organics were assumed not to be hygroscopic. Assuming some hygroscopicity for organic aerosols would enhance the difference between measured and modeled $b_{scat}(RH)/b_{scat,dry}$ ratios.

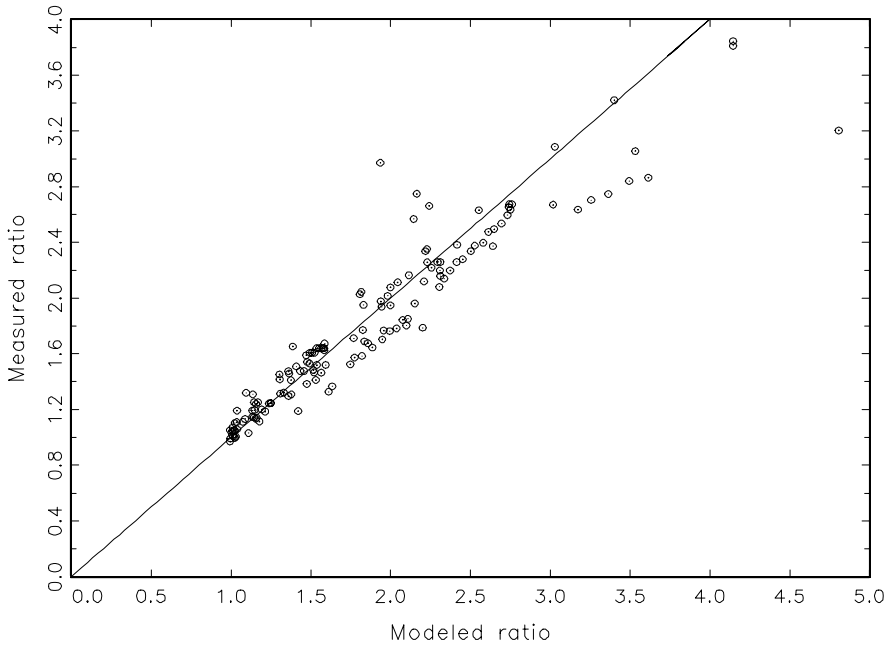

Figure 6.11 *Scatter plot of measured vs modeled $b_{scat}(RH)/b_{scat,dry}$ for the external mixture-variable sulfate size ($b_{scat}\_E\_e_s\_S_a\_B$) calculation. For reference the 1:1 line is also shown.*

Table 6.4 *Summary of ordinary least square regressions of measured and estimated $b_{scat}(RH)/b_{scat,dry}$ as the dependent and independent variables, respectively.*

Model	Intercept	Std error	Estimate	Std error	t-value	N	R^2
$b_{scat}\_E\_e_c\_S_a\_f(RH)$	0.31	0.023	0.79	0.012	0.000	368	0.92
$b_{scat}\_E\_e_s\_S_a\_B$	0.29	0.048	0.83	0.023	0.000	148	0.89
$b_{scat}\_M\_e_s\_S_a\_B$	0.43	0.079	0.82	0.042	0.000	148	0.71

Table 6.5 further summarizes the difference between the three model calculations. The numbers 1, 2 and 3 refer to averages of the differences over three relative humidity ranges

corresponding to 20-35%, 40-60%, and 75-95%. In all cases, the differences between the three models are accentuated at higher relative humidities with the external models yielding, in all cases, higher $b_{scat}(RH)/b_{scat,dry}$ ratios. The mean difference between external models is less than 1% for low RH values and only 3% at higher relative humidities. Differences between the internally mixed and external models is again small at low RH values and approach a mean difference on the order of 10% at the higher relative humidities. The maximum difference between the internally mixed and external models is about 30% for the 75-95% relative humidity range.

Table 6.5 *A summary of the percent differences between model estimations of $b_{scat}(RH)/b_{scat,dry}$ for three ranges of relative humidities. Number 1 refers to an average of $b_{scat}(RH)/b_{scat,dry}$ values between 20-35% RH, number 2 to average ratios between 40-60% RH, and number 3 to ratios between 75-95% RH.*

Variable	Number	Mean	Std. Dev.	Variance	Minimum	Maximum	N
$(b_{scat}\_M\_e_s\_S_a\_B)$ -	1	-0.60	0.60	0.36	-2.29	0.59	45
$(b_{scat}\_E\_e_s\_S_a\_B)$	2	-2.44	2.78	7.71	-9.55	3.26	45
	3	-6.91	8.24	67.83	-26.37	9.43	45
$(b_{scat}\_E\_e_c\_S_a\_f(RH))$ -	1	0.40	0.27	0.07	-0.05	1.20	45
$(b_{scat}\_E\_e_c\_S_a\_B)$	2	1.06	0.86	0.74	-0.30	4.70	45
	3	2.90	3.24	10.52	-0.97	16.78	45
$(b_{scat}\_M\_e_s\_S_a\_B)$ -	1	-1.00	0.71	0.50	-2.23	0.53	45
$(b_{scat}\_E\_e_c\_S_a\_f(RH))$	2	-3.51	2.79	7.76	-9.83	3.56	45
	3	-9.80	8.22	67.58	-29.17	10.39	45

6.1.4 Summary of the Great Smoky Mountains Study

The objective of calculations presented in this section were not to apportion scattering to any particular species but to examine the ability of various models to predict scattering of fine particles less than 2.5 μm both as a function of relative humidity and at ambient humidities. From these calculations it is possible to develop a better understanding of the sensitivity of scattering models to aerosol mixing assumptions, sulfate acidity, and the hygroscopic characteristics of various aerosol types.

A variety of aerosol scattering models was exercised. First, an externally mixed aerosol model where constant dry specific scattering was assumed, sulfate mass is assumed to be in the form of ammonium bisulfate and a functional dependence of scattering on relative humidity (RH), which was based on laboratory measured ammonium bisulfate growth, was used. Second, an external model with constant dry specific scattering was used but sulfate mass and changes in scattering efficiency due to growth as a function of relative humidity were accounted for as functions of sulfate ammoniation. Third, an externally mixed aerosol model was assumed, but with explicit incorporation of sulfate size and sulfate ammoniation with associated growth as a function of relative humidity accounted for. Finally, an internally mixed aerosol model that incorporated sulfate size, ammoniation, and associated sulfate hygroscopic growth was exercised. In all cases, only sulfates and nitrates were assumed to be hygroscopic.

When comparing model performance as it relates to predicting ambient scattering, the first and simplest model, which assumed only one type of sulfate species and constant dry specific scattering, performed the poorest. It predicted ambient scattering adequately at low scattering values but underpredicted scattering under high sulfate concentrations by about 30%. When the estimated mass of the sulfate species was corrected for its degree of ammoniation, model performance was improved substantially, and was further improved by estimating absorbed water as a function of sulfate ammoniation. Only slight improvement in model performance was achieved by explicitly accounting for variation in dry specific scattering coefficients due to changes in particle size distribution. The overall performance of the externally mixed model, with sulfate ammoniation, growth as a function of relative humidity and size, was excellent in that the averages between measured and predicted scattering were within 9% of each other, and an OLS regression between the two variables yielded an R^2 of 0.94. The effect of assuming the crystallization, deliquescent or best estimate branches of the sulfate growth curves was also explored. Each was used in the reconstructed scattering and it was shown that there were only small differences between the three estimations. The scattering associated with the crystallization curve was almost the same as the best estimate, while scattering calculated using the deliquescent curve was about 3% less than the best estimate.

For the internally mixed model, it was assumed that sulfates, nitrates, and organics were uniformly mixed, with nitrates, sulfates and organics all having the measured sulfur mass size distribution and soil mixed externally. The growth of the internally mixed particle was calculated using the ZSR assumptions with D/D_o as a function of RH set equal to 1 for organics, while nitrates were assumed to have the same hygroscopicity as sulfates. D/D_o for sulfate species was calculated using the "best estimate" growth curve. In general, the difference between the internal and external case is small. The average difference between the two calculations is only about 8%, with the internally mixed model yielding the higher reconstructed scattering estimates.

Comparison between measured and modeled $b_{scat}(\mathrm{RH})/b_{scat,dry}$ ratios were carried out using three of the four modeling approaches. Models used for the comparison were external with constant specific scattering but with sulfate ammoniation and associated growth accounted for, external with sulfate size, ammoniation, and growth incorporated, and the internally mixed model. In most cases, all three modeling approaches agreed well with each other, however, the ratios predicted by the internally mixed and external models under high relative humidity conditions differed from each other by as much as 30%, with the mixed model generally showing less increase in scattering with RH than the external models.

Measured ratios, in general, were well reproduced by all of the modeling approaches. The R^2s between measured and modeled ratios varied from 0.92 to 0.71 with the external models having the highest R^2. All models yielded ratios that were on the average, about 20% greater than those that were measured. The largest discrepancies occurred when organic mass concentrations were highest with modeled ratios being greater than those measured.

6.2 GRAND CANYON STUDIES

Two other studies were carried out at Grand Canyon, Arizona. National parks on the Colorado Plateau experience some of the best visibility in the continental United States. Annual average extinction, including Raleigh scatter, is about 31 1/Mm in the inner-mountain western United States as compared to rural eastern sites where the average extinction is near 130 1/Mm. In the eastern United States and at parks such as the Great Smoky Mountains, sulfates contribute most of the visibility degradation, whereas on the Colorado Plateau extinction is more evenly split between sulfates that make up about 23% of total extinction and carbon (scattering plus absorption), which may be as high as 33% depending on how absorption is estimated. About 10% of extinction is estimated to be associated with soil and coarse mass [Sisler, 1996; Malm et al., 1994]. While the fraction of extinction associated with sulfates is expected to decrease in the next two decades as a result of projected decreases in sulfur dioxide emissions, carbon emissions are expected to increase as prescribed fire activity by federal land managers is projected to increase by factors of 5-10 [Sandberg et al., 1979].

The accurate estimation of b_{abs} and coarse mass scattering remain problematic. Absorption can be estimated by assigning a mass absorption efficiency to elemental carbon or it can be estimated from direct measurements of light attenuation as it passes through a filter medium on which the absorbing material has been collected. Horvath [1993] reviewed the various filter absorption measurement techniques and concluded that, depending on scattering albedo and filter loading, measured absorption values are too high by factors on the order of 20-80%! Presumably, the overestimation of absorption is due to multiple scattering effects and/or light leakage from the edge of the filter medium. On the other hand, Eldred and Cahill [1994] clearly showed that absorption estimates decrease as filter aerial density increases. They collected multiple samples over the same time period but with different filter "masks" that results in varying aerial densities. Absorption, derived from the various filters with varying aerial density, showed a decrease as aerial density increased when absorption estimates should have been the same. These series of measurements suggest that absorption estimates based on filter transmittance underpredict by as much as a factor of two, depending on filter loading. They suggest that a fraction of absorbing particles were "shadowed" by nearest neighbors masking or blocking light from particles below the outermost particle layers.

Hitzenberger et al. [1999] compared a number of commonly employed absorption measurement techniques and showed that, even though all techniques were highly correlated, the absorption estimates varied by more than factors of two. Furthermore, mass absorption efficiencies have been reported in the literature that range from about 5–20 m^2/g [Horvath, 1993] with a value of 10 m^2/g being used by most researchers in the field. It is interesting to point out that Fuller et al. [1999], in a theoretical exploration of elemental carbon scattering and absorption as a function of elemental carbon physical characteristics and mixing assumptions, were unable to justify absorption efficiencies for elemental carbon as high as 10 m^2/g. They concluded that efficiencies in the range of 5-8 m^2/g were more likely.

In the IMPROVE monitoring network, elemental carbon (EC) is measured using the thermal optical reflectance (TOR) technique [Chow et al., 1993] and b_{abs} has been estimated using a laser integrated plate method (LIPM) and more recently with a hybrid integrating plate and sphere

(HIPS) instrument [Campbell et al., 1997]. Both measurements have been made on rather heavily loaded (more than a monolayer of deposit) Teflon filters. Absorption estimates using LIPM and HIPS are further corrected for aerial density effects, discussed above, that results in an upward scaling of about a factor of 1.7-2.0. Interestingly, comparison of b_{abs} derived from HIPS and corrected for variation in aerial density and 10*EC shows the b_{abs} measurement to be about a factor of two higher than absorption estimated from elemental carbon.

Malm et al. [1996], using IMPROVE data, compared reconstructed extinction with measured extinction and concluded that absorption estimated by LIPM and corrected for aerial density was needed to achieve closure between the two variables. Using 10*EC as the absorption estimate for reconstructing extinction fell short of measured extinction. On the other hand, one could use 10*EC as the absorption estimate and increase coarse mass scattering and achieve closure with about the same degree of accuracy as using b_{abs} as determined by LIPM. Together absorption and coarse mass scattering make up about 30-50% of aerosol extinction in the western United States [Malm et al., 1996; Sisler, 1996].

There has been very little work investigating coarse particle scattering. The value most often used for coarse scattering efficiency is 0.6 m^2/g, a value that was originally reported by Trijonis [1988] for a study carried out in the Mojave Desert, while White [1990] reported coarse mass scattering efficiencies of 0.34-0.45 m^2/g for data collected near Lake Mead and White and Macias [1990] reported a value of 0.4 m^2/g for data collected at Spirit Mountain, which is about 100 miles south of Las Vegas, Nevada. The inlet size cut (D_{aero}) for the coarse mode for the White [1990] and White and Macias [1990] studies was 15 μm, while the Trijonis [1988] study reported on data collected with an inlet corresponding to D_{aero}<10 μm. All these studies occurred in desert areas where dust can contribute as much as 50% of the particle extinction budget. Estimates of coarse mass scattering have not been made in other nonurban areas of the United States.

In part, it is the inability to conclusively apportion about 30-50% of the extinction budget between coarse mass scattering and particle absorption that has motivated the measurement program reported here. To investigate these issues a study was carried out from July 10, 1998 through August 8, 1998 on the south rim of Grand Canyon National Park.

Experiments were designed such that observables could be estimated or modeled in a number of different ways. Fine mass was gravimetrically determined for both D_{aero} < 10 and 2.5 μm, which can be compared to reconstructed mass based on measured species. Dry and ambient 2.5 μm scattering was measured, which in turn can be compared to reconstructed scattering based on aerosol species measurements. Open-air nephelometry was used to measure ambient scattering of fine and coarse particles that can be used to estimate coarse particle scattering, which in turn can be used with extinction measurements to develop independent estimates of absorption. Fine and coarse mass absorption was independently measured using two filter substrates and with an aethalometer. Scattering as a function of relative humidity was also measured with a humidograph allowing for estimates of $f(\mathrm{RH}) = b_{scat(wet)}/b_{scat(dry)}$, which in turn can be used to develop estimates of aerosol growth. Modeling ambient scattering and the wet-to-dry scattering ratio will serve to both explore the validity of aerosol growth and mixing models and associated assumptions, and provide an estimate of the hygroscopicity of aerosol species

other than sulfates and nitrates. The following discussion will focus on exploring the scattering properties of fine and coarse particulates under ambient conditions and particle absorption.

6.2.1 Experimental Methods

The details of the nephelometer and particle measurement program were discussed previously on the special study at Great Smoky Mountains.

6.2.1.1 Transmissometer

Transmissometers are calibrated to measure the irradiance, at 550 nm, of a light source after the light has traveled over a finite atmospheric path. The transmittance of the path is calculated by dividing the measured irradiance at the end of the path by the calibrated initial intensity of the light source. The average extinction of the path is calculated using Bouger's law from the transmittance and length of the path. The measurement is ambient in that air samples are not passed through an enclosed chamber.

Transmissometers employed in this study are the Optec, Inc., LPV-2 instruments, which have been in operation since 1986. Their use in remote locations such as national parks is discussed by Molenar *et a1*. [1989], while their use in urban settings is presented by Dietrich et al. [1989]. Careful operation of the transmissometer (daily cleaning of optics and pre and post calibrations) should result in extinction measurements with an accuracy of about 10% [Molenar *et a1*., 1989]. The transmissometer was located near the particle samplers but on the rim of the canyon. Therefore, the separation between the transmissometer and all other instruments was about 1.5 km.

6.2.1.2 Aethalometer

The aethalometer collects aerosol continuously on a quartz fiber filter, while measuring the optical transmittance through the filter [Hansen et al., 1982]. The rate of decrease of optical transmittance as a function of the rate of increase of filter loading has been found to be proportional to the atmospheric absorption. The aethalometer can be operated at a flow rate of 5-10 l/min and is purported to have an accuracy of about 10%. Its sample air was extracted from a sampling plenum that was also fitted with a 2.5 μm cyclone inlet.

6.2.2 Summary of Measurements

Table 6.6 summarizes the optical measurement in the form of mean, standard deviation, minimum, and maximum. The number of valid data points is also given. The extinction measurements, b_{ext}, were made with a transmissometer, while $b_{scat,open}$, $b_{scat,2.5\mu m}$, and $b_{scat,dry}$ refer to scattering measurements made with the open air nephelometer, the nephelometer fitted with a 2.5 μm inlet, and the nephelometer designed to operate with an inlet that dried the aerosol, respectively. The absorption measurement, $b_{abs,2.5\mu m}$, referred to in this table, was made with the aethalometer fitted with a 2.5 μm inlet. RH_{neph}, and RH_{trans} refer to the relative humidity measured at the nephelometer and transmissometer locations.

As a quality assurance check, the $b_{scat,dry}$ values derived from the Radiance Research nephelometer, which was run with an aerosol drying system, was compared to the Optec nephelometer derived scattering, which operated under ambient relative humidity conditions, when the relative humidity was less than 45%. For nearly neutralized sulfate aerosols, one would not expect significant growth below 45% relative humidity at Grand Canyon [Zhang et al., 1994]. Figure 6.12 shows the comparison for a 100 min averaging time along with the 1:1 line (R^2=0.92). The difference between the average scattering coefficients for the data presented in Figure 6.12 is less than 5% at 6.9 1/Mm and 6.5 1/Mm for the Radiance Research and Optec nephelometers, respectively.

Table 6.6 *Statistical summary of ten-minute optical and relative humidity measurements. The scattering and extinction values include Rayleigh scattering.*

Variable	Mean (1/Mm)	Std. Dev.	Minimum (1/Mm)	Maximum (1/Mm)	Valid
b_{ext}	23.06	11.23	7.70	192.8	6432
$b_{scat,open}$	20.59	6.62	8.40	63.00	5660
$b_{scat,2.5\mu m}$	18.03	7.96	7.80	86.80	6052
$b_{scat,dry}$	16.23	3.71	9.38	35.07	5875
$b_{abs,2.5\mu m}$	1.12	1.26	-3.33	46.27	6762
RH_{neph} (%)	42.39	25.32	5.73	100.00	6843
RH_{trans} (%)	34.56	22.35	4.46	97.80	6762

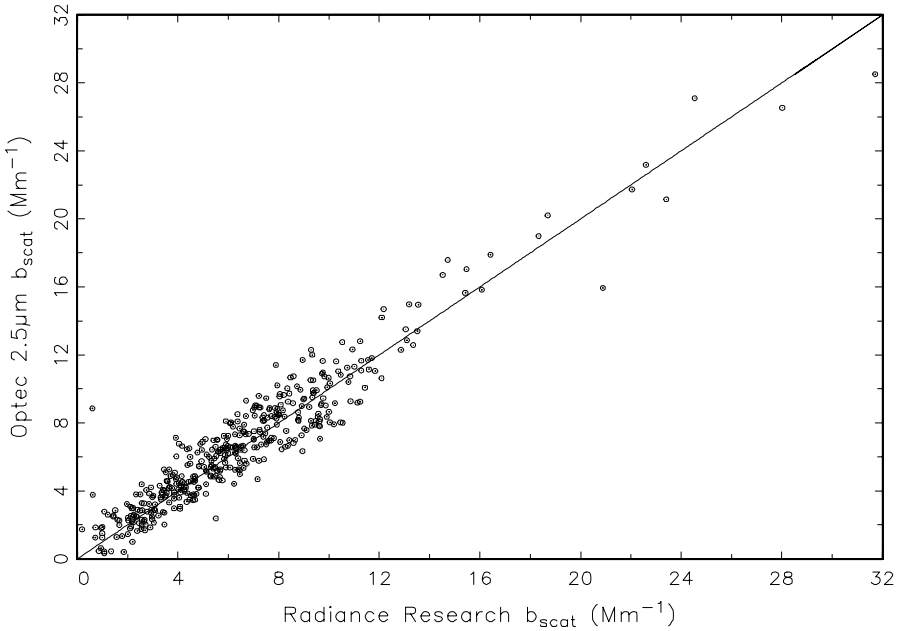

Figure 6.12. *Scatter plot of b_{scat} measured by the Radiance Research and Optec nephelometers for relative humidities less than 45%. The 1:1 line is shown for reference. Both instruments were fitted with a 2.5 µm cyclone inlet.*

A number of authors [Heintzenberg and Quenzel, 1973; Fitzgerald, 1977; Hasan and Lewis, 1983; Sloane et al., 1990] estimated that the MRI series of nephelometers see about half of the actual scattering from representative distributions of coarse particles because of large angle truncation errors (the MRI nephelometers integrated over angles between 8 and 168 degrees). White et al. [1994] used field measurements obtained in the Subregional Cooperative Electric Utility National Park Service, and Environmental Protection Agency Study (SCENES) [McDade and Tombach, 1987] to independently estimate the fraction of coarse particle scattering measured by these nephelometers. They regressed total scattering (b_{ext}-b_{abs}) against fine and coarse particle scattering as measured by the 1597 MRI integrating nephelometer fitted with and without a 2.5 μm cyclone inlet. The regression coefficient on coarse particle scattering was 2.3±13% consistent with the theoretically estimated factor of two.

Molenar [1997] carried out similar theoretical calculations of the expected underprediction of coarse particle scattering associated with the Optec nephelometer and showed that at 550 nm it will underestimate coarse particle scattering by 5-30%, depending on assumed particle size distributions.

Referencing Table 6.6, b_{ext} exceeds $b_{scat,2.5\mu m}$ by about 5 1/Mm or 37% of aerosol extinction, a significant fraction of the extinction budget. If the open air nephelometer indeed does measure most of the coarse particle scatter and most of the absorption is due to particles less than 2.5 μm, then $b_{ext} \cong b_{scat,open} + b_{abs,2.5\mu m}$. The sum of $b_{scat,open}$ and $b_{abs,2.5\mu m}$ is 21.7 1/Mm or about 1.35 1/Mm short of measured extinction. One could achieve closure if it is assumed that the aethalometer measurement of $b_{abs,2.5\mu m}$ is about 2.2 times underestimated or about 2.47 1/Mm instead of 1.12 1/Mm. On the other hand, the difference between the open air and fine particle (D_{aero}<2.5 μm) scattering is 2.56 1/Mm and is presumably associated with coarse particle scattering. Assuming for the moment that this value is one half of coarse particle scattering one can estimate coarse particle scattering to be 5.12 1/Mm. Then coarse plus fine particle scattering alone would be 23.15 1/Mm, which is very close to measured extinction without including absorption.

The degree to which absorption and/or coarse particle scattering are over or underestimated can be explored using regression analysis. Assuming that $b_{scat,open}$-$b_{scat,2.5\mu m}$ is proportional to coarse particle scattering and b_{ext}-$b_{scat,2.5\mu m}$ is coarse particle scattering plus absorption of both coarse and fine particles one can write the following equation:

$$(b_{ext} - b_{scat,2.5\mu m})_i = a_o + a_1(b_{scat,open} - b_{scat,2.5\mu m})_i + a_2(b_{abs,2.5\mu m})_i \qquad (6.7)$$

where i refers to the i^{th} sampling period and a_o, a_1, and a_2 are constants. This series of equations can be solved using ordinary least square (OLS) regression analysis.

Figure 6.13 shows the temporal plot of b_{ext} and $b_{scat,2.5\mu m}$ for 10.0 min time intervals starting at JD 161 and ending on JD 210 (June 10 – August 29). In most cases, the two variables co-vary with each other, however, during some time periods they are actually anti-correlated. For reference, the overall correlation is 0.62, while the correlation between two collocated samplers, $b_{scat,open}$ and $b_{scat,2.5\mu m}$ is 0.93. The insert in Figure 6.13 shows a time period from JD 181-183 where the variables are almost exactly out of phase with each other. The reader is reminded that

the transmissometer measurement is path averaged over 5 km and is about 1.5 km distant from the nephelometers.

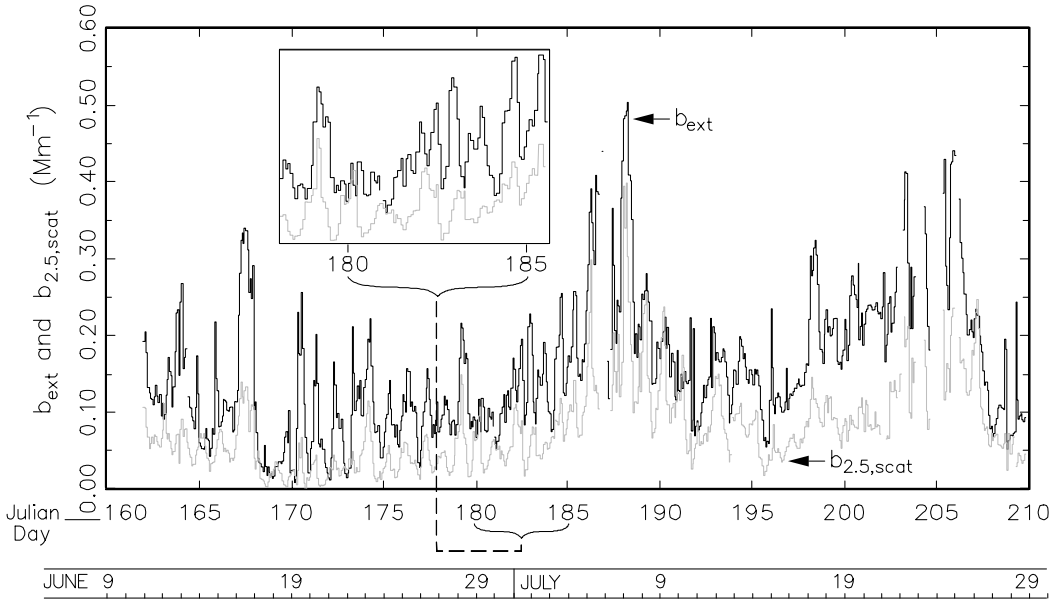

Figure 6.13 *Temporal plot of measured extinction and scattering by particles less than 2.5 μm. The time increment associated with each data point is 10 minutes.*

For purposes of the regression analysis, short temporal variability in the data was minimized by averaging to 16 hrs and requiring that the 16-hr data have at least 8 hrs of nonmissing values. Furthermore, because the relative humidity at the transmissometer site was lower than at the nephelometer location, only optical parameters were included in the averaged data set if the relative humidity was less than 60%. Figure 6.14 is a temporal plot of the averaged b_{ext}, $b_{scat,2.5\mu m}$, and $b_{abs,2.5\mu m}$ values.

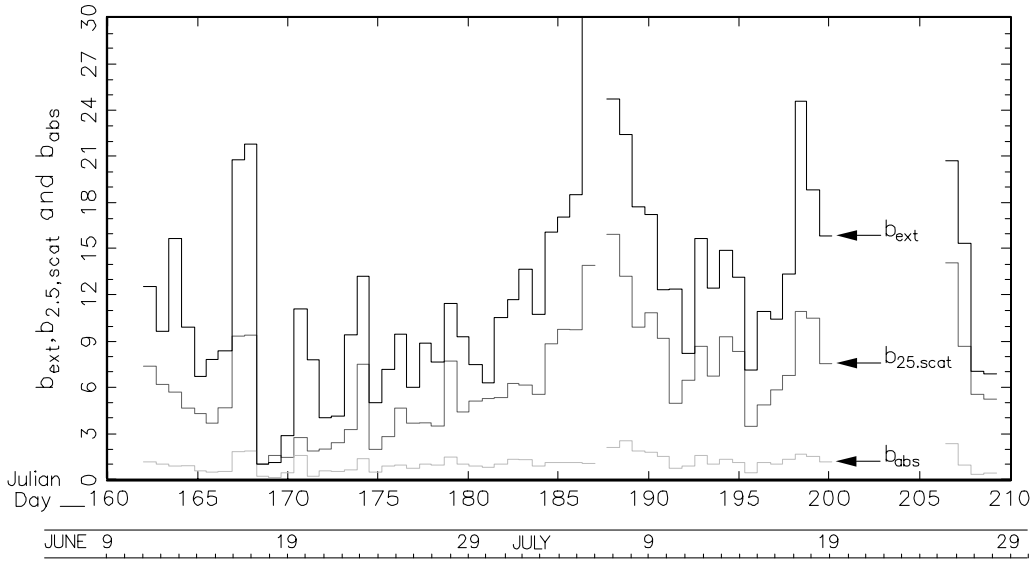

Figure 6.14 *Temporal plot of measured extinction, scattering and absorption by particles less than 2.5 μm for 16-hr time intervals*

Table 6.7 shows the results of the regression. The regression coefficients are highly significant with standard error for both coefficients being about 20%. Figure 6.15 is a scatter plot of reconstructed and measured extinction where reconstructed extinction is based on the regression coefficients presented in Table 6.7. For comparison the 1:1 line is also shown and R^2=0.87.

The coefficient associated with coarse particle scattering as determined by the nephelometers ($b_{scat,open}$-$b_{scat,2.5\mu m}$) suggests that coarse particle scattering is overestimated by about 18±19%. On the other hand, the coefficient associated with $b_{abs,2.5\mu m}$ implies that measured absorption is low by a factor of about 2.8±0.62! Changing the averaging time does alter the coefficients somewhat. For instance, for an averaging time of an hour the coefficient on coarse particle scattering remains unchanged and its significance level increases but the coefficient associated with absorption is reduced from 2.76 ±0.62 to 1.6 ± 0.35. However, the overall model R^2 is decreased to 0.36.

Table 6.7 *Summary of OLS regression with b_{ext}-$b_{scat,2.5\mu m}$ as the dependent variable and $b_{scat,open}$-$b_{scat,2.5\mu m}$, and $b_{abs,2.5\mu m}$ as independent variables. $b_{abs,2.5\mu m}$ refers to aethalometer measurements in this table.*

Valid cases: 49	Dependent variable: b_{ext}-$b_{scat,2.5\mu m}$			R^2=0.60	
Variable	Estimate	Std error	t-value	Prob t>|t|	Cor dep var
intercept	-0.0004	0.0007	-0.59	0.56	-------
$b_{scat,open}$-$b_{scat,2.5\mu m}$	0.82	0.19	4.27	0.00	0.67
$b_{ath,2.5\mu m}$	2.76	0.62	4.44	0.00	0.68

Because the nephelometers and transmissometer are not sampling the exact same air mass, the regression analysis should be viewed as semi-quantitative. However, the analysis strongly suggests that fine particle absorption as measured by the aethalometer is an underestimate of total absorption. The "calibration" factor for the aethalometer could be in error or there may be substantial coarse particle absorption.

6.2.3 Summary of Particulate Measurements

A statistical summary of fine and coarse particle (PM_{10}-$PM_{2.5}$) concentrations are presented in Table 6.8, while temporal plots are shown in Figures 6.16 and 6.17 for coarse and fine mass components, respectively. Organics (H) and organics (C) refer to organic mass estimates based on hydrogen and carbon, respectively. Because only module A was used to sample PM_{10} analysis is limited to PIXE, XRF, and PESA. Therefore, coarse carbon and nitrates cannot be explicitly determined and coarse organics must be estimated using Equation (6.8).

$$OCH = 11(H - 0.25S) \tag{6.8}$$

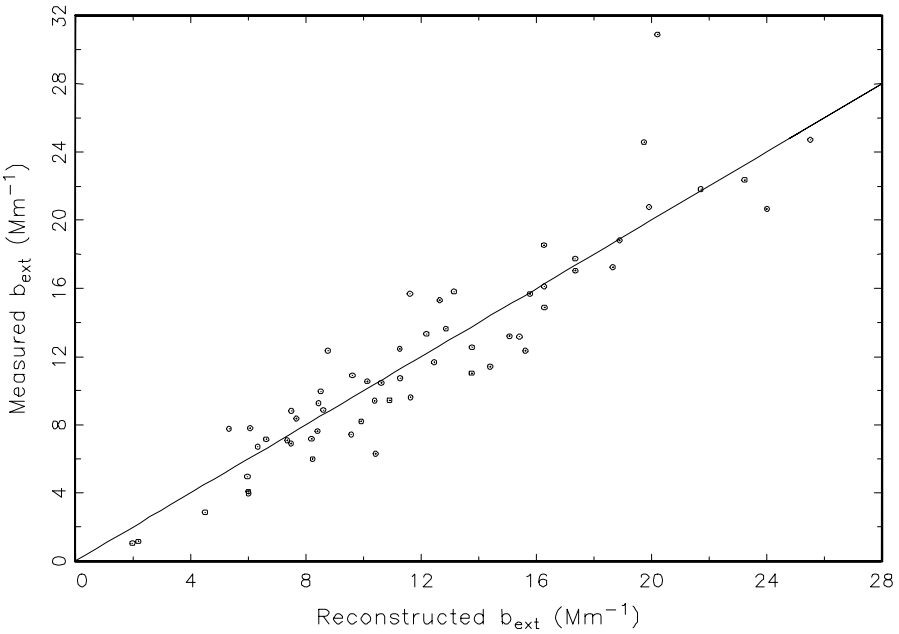

Figure 6.15 *Scatter plot, along with the 1:1 line, of measured and reconstructed extinction.*

Table 6.8 *Statistical summary of aerosol measurements.*

Variable	**Mean ($\mu g/m^3$)**	**Std. Dev. ($\mu g/m^3$)**	**Minimum ($\mu g/m^3$)**	**Maximum ($\mu g/m^3$)**	**Valid**
Coarse Mass	5.71	4.39	0.97	22.80	37
Coarse $(NH_4)_2SO_4$	0.14	0.13	0.00	0.44	37
Coarse organics (H)	2.70	1.54	0.64	7.30	37
Coarse Soil	4.14	4.30	0.27	24.31	37
	(3.06)	(3.18)	(0.20)	(17.99)	
Fine Mass	3.88	1.20	1.79	6.55	37
Reconstructed Fine Mass	3.68	1.05	1.67	6.02	37
$(NH_4)_2SO_4$	1.27	0.67	0.21	2.74	37
Organics (C)	1.52	0.42	0.64	2.18	37
Organics (H)	1.57	0.53	0.85	3.26	37
Elemental Carbon(EC)	0.10	0.08	-0.04	0.26	37
NH_4NO_3	0.20	0.12	0.03	0.55	37
Fine Soil	0.60	0.24	0.25	1.28	37

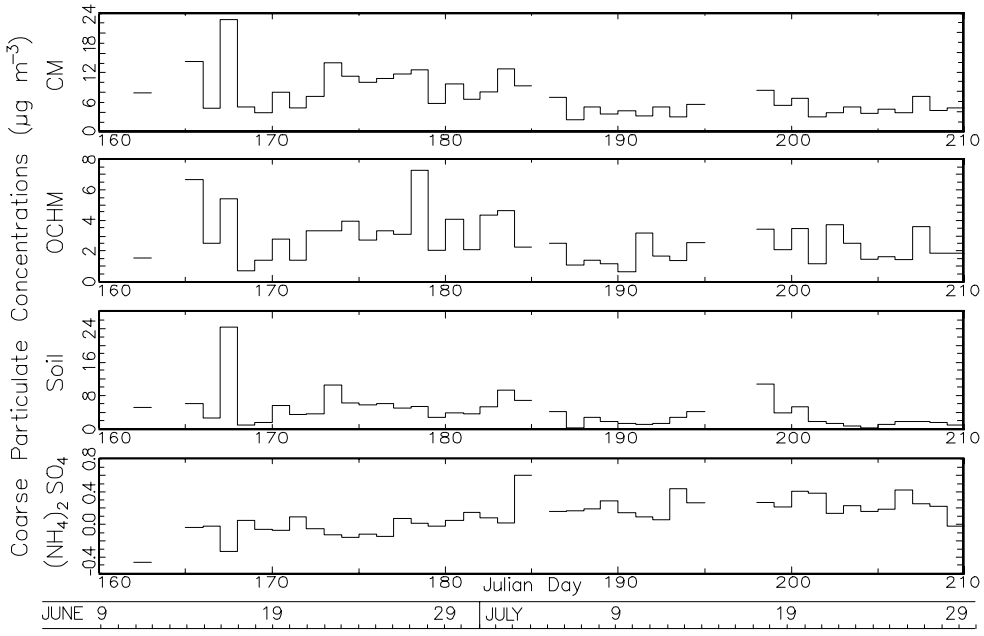

Figure 6.16 *Temporal plot of coarse particle (PM_{10}–$PM_{2.5}$ µm) concentrations. CM refers to gravimetric coarse mass and OCHM to organics by hydrogen.*

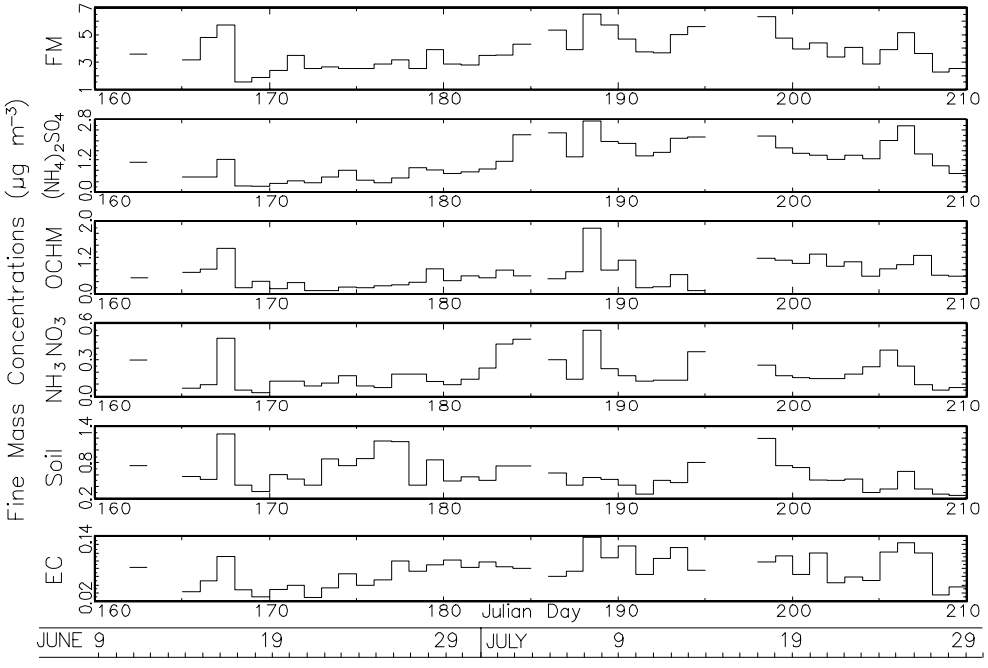

Figure 6.17 *Temporal plot of fine particle concentrations. FM refers to gravimetric fine mass, while OCHM is organics by hydrogen.*

Gravimetric coarse and fine mass on the average are about equal at 5.71 and 3.88 μg/m^3, respectively. Reconstructed and gravimetrically determined fine mass compare favorably at 3.88 and 3.68 μg/m^3, respectively, however, one can see that the sum of coarse mass constituents, without including elemental carbon and nitrates, are an overestimate of measured coarse mass. The sum of average coarse organics and soil alone are 6.84 μg/m^3, while measured average coarse mass is 5.71 μg/m^3. Apparently, the algorithms that have been developed for estimating fine mass constituents yield overestimates for their coarse counterparts.

To explore the degree to which coarse soil and organics are overdetermined, a regression analysis was carried out with CM as the dependent variable and coarse OCHM, ammonium sulfate, and soil as independent variables. The results are presented in Table 6.9. Sulfate concentrations are low and its coefficient is not statistically significant. The coefficient of determination (R^2) is high at 0.80 and the statistical significance of the coefficients associated with soil and OC are high. The regression results suggest that soil is overdetermined by 26%, while organic estimates are approximately correct. Table 6.8 also includes, parenthetically, coarse soil concentrations that have been corrected to the regression results (multiplied by 0.74).

Table 6.9 *Summary of results of an ordinary least square (OLS) regression with coarse mass as the dependent variable and soil and organics as the independent variables.*

Valid cases: 43	Dependent variable: CM			R^2=0.80	
Variable	Estimate	Std error	t-value	Prob t>|t|	Cor dep var
Soil	0.74	0.06	12.10	0.00	0.95
OC	1.00	0.12	8.42	0.00	0.91

Figure 6.18 shows a scatter plot of reconstructed and gravimetric fine mass along with a 1:1 line. The data points are scattered around the 1:1 line and the coefficient of determination for an OLS regression between the two variables is 0.78.

Referring to Table 6.8, organics are the largest fraction of fine mass, while soil is the largest fraction of coarse mass. Sulfates make up a small to negligible contribution to the coarse mode, while they are the second largest contributor to fine mass. Organics also contribute significantly to coarse mass. Referring to Figures 6.16 and 6.17, a number of interesting episodes present themselves. On JD 167 there was a coarse mass episode that reached 23 μg/m^3, while the corresponding fine mass concentration was about 6 μg/m^3. The coarse mode was made up primarily of soil but with a significant amount of organics present. In the fine mode, dust is also a large contributor at 1.28 μg/m^3 but organic concentrations are slightly higher at 1.47 μg/m^3 and sulfates are 1.22 μg/m. On JD 165, CM has the second highest value and coarse soil and organics are approximately equal with organics being slightly higher. Fine mass is not particularly high on that day. Coarse mass tends to be the highest during the early part of the sampling period (JD 160 to 188), while fine mass, other than the "dust" episode just discussed, was highest in the latter half of the study period (JD 188 to 210).

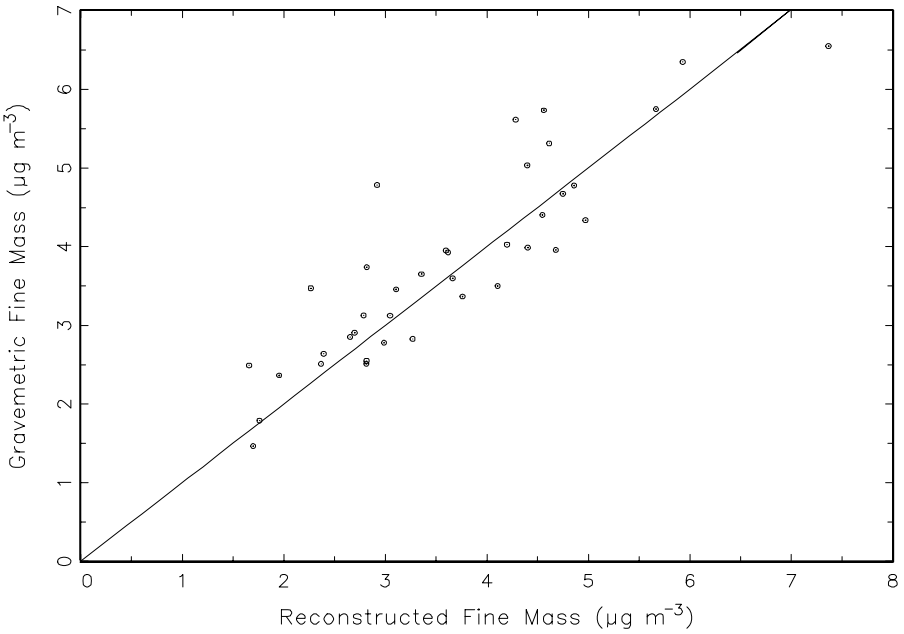

Figure 6.18 *Scatter plot, along with the 1:1 line, of measured and reconstructed fine mass.*

6.2.4 Estimates of Coarse Mass Scattering Efficiencies

Within the uncertainty of the regression analysis as defined by Equation (6.7), $b_{scat,open}$ - $b_{scat,2.5\mu m}$ gives an estimate of coarse particle scattering. Therefore, large particle scattering efficiency can be estimated by:

$$e_{CM} = (b_{scat,open} - b_{scat,2.5\mu m}) / CM. \tag{6.9}$$

From a physical perspective, $b_{scat,open}$ -$b_{scat,2.5\mu m}$ should be an underestimate of coarse particle scattering in that $b_{scat,open}$ undermeasures scattering due to all particles and therefore e_{CM} would be underestimated. Figure 6.19 is a scatter plot of coarse particle scattering efficiency (e_{CM}) and CM. Scattering efficiency is in units of m^2/g, while CM is in $\mu g/m^3$. The horizontal line corresponds to a scattering efficiency of 0.6 m^2/g, which is the "best estimate" suggested by Trijonis et al. [1990]. The lowest scattering efficiencies reported in the literature (0.34-0.45 m^2/g) were derived from measurements at Meadview during the SCENES study [White et al., 1994].

Referring to Figure 6.19, one can see that for CM mass concentrations above about 8.0 $\mu g/m^3$ estimated scattering efficiencies are consistent with the above referenced studies. However, for lower coarse mass concentrations efficiencies vary between about 0.5 and 1.2 m^2/g. Coarse mass efficiencies (e_{CM}) even as high as 0.6 m^2/g are hard to justify on a theoretical basis and to have mass scattering efficiencies as high as 1.0 m^2/g are even more difficult. For instance, assuming coarse soil has a mass median diameter (d_g) of 4.0 µm, geometric standard deviation (σ_g) of 2.0, index of refraction of 1.53, and density of 2.3 g/cm^3

yields a coarse mass scattering efficiency of about 0.35 m^2/g. Efficiencies as high as 0.6 m^2/g occur only when coarse soil particle mass mean diameters are near the 2.5 μm cyclone cut point.

Coarse mass scattering efficiencies as high as 1.0 m^2/g can occur if, as stated above, coarse soil mass size distributions are shifted to near the cyclone cut point, coarse particles are made up of other species that are less dense and therefore scatter more light on a per mass basis. The data does, to some degree reflect, these hypotheses. The highest coarse mass scattering efficiencies occur when the ratio of fine to coarse soil is greatest (0.4), and when this ratio is low (0.1-0.2), e_{CM} is lowest at about 0.4 m^2/g. Furthermore, the higher coarse mass efficiencies also occur when organics are the larger fraction of coarse mass and on the other hand when coarse organics make up only about 20% of the coarse mass the efficiencies drop to about 0.4 m^2/g.

A source of error in the above estimation of e_{CM}, is that the open-air nephelometer could be potentially biased from particles larger than 10.0 μm and therefore Equation (6.9) would necessarily be an overestimation of scattering by particles in the 2.5-10.0 μm range. Another potential source of error in the above estimation of e_{CM} is large particle (>2.5μm) "leakage" by the cyclone onto the PM2.5 substrates. CM estimates (PM_{10}-$PM_{2.5}$) would then be biased low and, therefore, CM scattering efficiencies biased high.

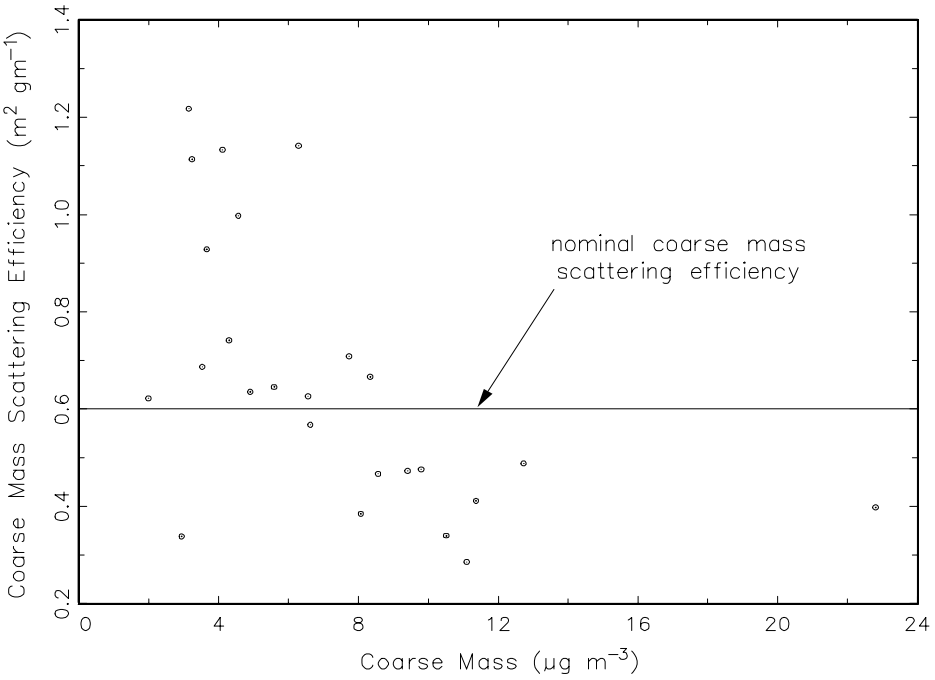

Figure 6.19 *Scatter plot of coarse mass scattering efficiency as a function of coarse mass concentration. The horizontal line corresponds to the mass coarse particle mass scattering efficiency that is typically used as a nominal value.*

6.2.5 Absorption Estimates

As sulfate concentrations decline, as a result of reduction in sulfur dioxide emissions, and organic and elemental carbon concentrations are projected to increase, as a result of increased urban populations and prescribed fire, the contribution of absorption to haze can be anticipated to increase. Yet there are no reliable means of estimating absorption. Most, if not all, absorption estimates rely on transmission measurements of aerosols collected on some filter media. Horvath [1993] reviewed many of these measurements. The absorption estimates are sensitive to the type of substrate used, optical configuration of the transmission measurement device, filter loading, and scattering albedo.

Arnott et al. [1999] developed a prototype photoacoustic spectrometer, which is undergoing initial field tests, while Moosmüller [1998] is developing an in-situ enclosed-folded path transmissometer that can be fitted with a size-selective inlet and thereby compared directly to nephelometers with size-selective inlets. Both instruments should go a long way toward resolving which of the many different filter type measurement schemes are most accurate.

In IMPROVE, absorption estimates have been derived from transmission measurements of the Module A Teflon filter using both LIPM and HIPS (see Section 6.2), while many other studies have employed a Nuclepore substrate. The aethalometer essentially makes a transmission measurement through a quartz type filter. In this field campaign, absorption estimates were derived by six different techniques: b_{lac} is 10 m^2/g * EC, $b_{ath,2.5\mu m}$ is the aethalometer measurement, LIPM is the laser integrated plate measurement on Teflon, HIPS is the hybrid integrated plate and sphere on Teflon, and NLIPM and NHIPS are the same measurements only on a Nuclepore substrate. CLIPM and CHIPS are coarse absorption derived from differencing PM_{10} and $PM_{2.5}$ LIPM and HIPS measurements on the associated Teflon filters.

Table 6.10 summarizes the absorption estimates. Not shown in Table 6.10 are the corrections for aerial density effects that have been routinely applied to LIPM and HIPS estimates. These corrections result in an upward scaling of about 1.7-2.0. It is interesting to note that the HIPS measurement, which is designed to compensate for filter reflectance effects, is lower than LIPM for Teflon filters but greater for Nuclepore substrates. The aethalometer and NLIPM, on the average, are within about 6% of each other and b_{lac} is about 30% greater than either of these two measurements. LIPM is about a factor of 2 greater than $b_{ath,2.5\mu m}$ or NLIPM, while HIPS is about a factor of 1.6 greater. Coarse absorption is on the order of about one half of fine absorption.

Figure 6.20 shows a multiple scatter plot of each of these variables scattered against each other. Each of the separate scatter plots will not be discussed as to how and why each variable is somewhat different than the next but are only included for completeness and for the interested reader. All variables are well correlated with each other but in some cases the differences between the variables are biased additively, while in other cases there is a multiplicative bias. For instance, LIPM has about a 1 1/Mm offset when compared to $b_{ath,2.5\mu m}$, while NHIPS when compared to $b_{ath,2.5\mu m}$ is lower by a multiplicative factor of about two. $b_{ath,2.5\mu m}$ and NLIPM compare the most favorably both on the average and across all values, while b_{lac} also compares

favorably with $b_{ath,2.5\mu m}$ and NLIPM. If the 1 1/Mm offset is subtracted from LIPM then it too compares well with $b_{ath,2.5\mu m}$, NLIPM, and b_{lac}. Finally, based on Figure 6.20, it is evident that coarse and fine absorption are correlated.

Table 6.10 *Statistical summary of absorption measurements.*

Variable	Mean (1/Mm)	Std. Dev. (1/Mm)	Minimum (1/Mm)	Maximum (1/Mm)	Valid
b_{lac}	1.38	0.68	0.07	2.56	21
$b_{ath,2.5\mu m}$	1.07	0.45	0.26	2.02	21
LIPM	2.19	0.63	0.92	3.69	21
HIPS	1.69	0.65	0.56	3.42	21
NLIPM	1.14	0.66	0.00	2.58	21
NHIPS	2.14	0.94	0.22	4.32	21
CLIPM	1.05	1.03	0.00	4.67	21
CHIPS	0.37	0.65	0.00	2.93	21

The solution of Equation (6.9) implies that absorption, as measured by the aethalometer, is an underestimate of absorption by an amount on the order of about 2. The regression coefficients, although quite significant, are sensitive to averaging time and in the broadest sense OLS type regressions are also sensitive to the inherent uncertainty of the measurements themselves [White, 1990]. It is further emphasized that the aethalometer measurements are for fine particle absorption, while b_{ext}-$b_{scat,2.5\mu m}$ is sensitive to fine and coarse particle absorption. LIPM measurements for coarse and fine particle absorption, after correcting for the 1/Mm fine particle offset (the correction isn't needed for coarse particle absorption because it is derived by differencing the PM_{10} and $PM_{2.5}$ absorption and the offset is thus subtracted out) are the same at about 1/Mm. Coarse particle HIPS is only 0.25 that of fine particle HIPS absorption.

Therefore, within the uncertainty of the analysis, regression results are consistent with absorption measurements. Total absorption, both fine and coarse, is on the order of about a factor of two greater than fine particle absorption by itself. Because the uncertainty of accurately measuring total absorption in the 1 to 3 1/Mm range by differencing optically derived variables (b_{ext}-$b_{scat,2.5\mu m}$ and $b_{scat,open}$-$b_{scat,2.5\mu m}$) the analysis should be viewed as semi-quantitative. It is clear, however, that total atmospheric absorption can be substantially underestimated if only fine particle absorption is considered.

Finally, a regression was carried out using:

$$b_{ath,2.5\mu m} = a_1(E1+E2) + a_2(O4+OP) + a_3(Soil) \tag{6.10}$$

where $b_{ath,2.5\mu m}$ is the absorption as determined using the aethalometer, E1, E2, O4, and OP are the carbon concentrations corresponding to the different temperatures over which carbon molecules are vaporized in the TOR technique [Chow et al., 1993], and Soil is fine particle soil. This type of analysis has been carried out by Huffman [1996] and Malm et al. [1996] but with $b_{abs,2.5\mu m}$ as determined by LIPM on Teflon and with the aerial density correction applied. In these previous analyses, absorption efficiencies associated with EC were on the order of 12 m^2/g

which, based on theoretical calculations, are unlikely unless rather severe assumptions are made concerning the density of elemental carbon [Fuller et al., 1999].

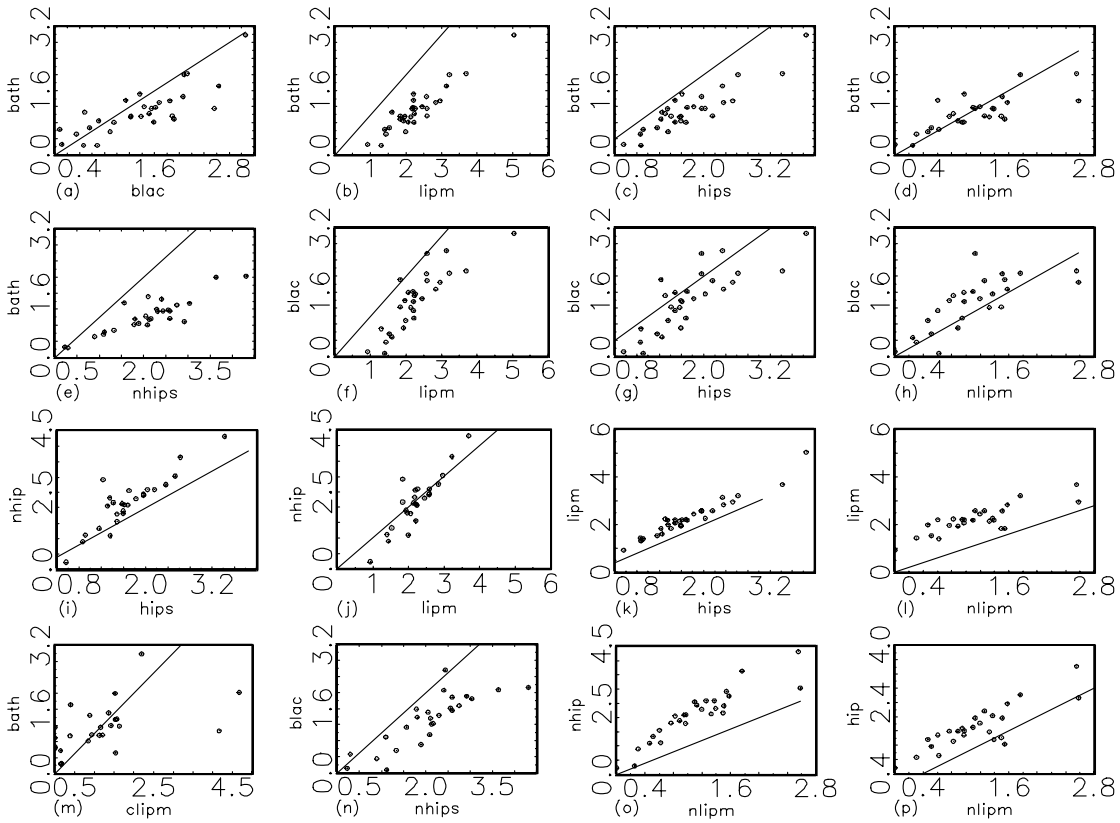

Figure 6.20 *Multiple scatter plots, along with 1:1 lines, of absorption measured in a number of different ways. lipm, hips, bath, and blac refer to laser integrated plate method, hybrid integrated plate and sphere instrument, aethalometer, and 10*EC where EC refers to elemental carbon, respectively. The lipm and hips measurements were made on Teflon, while nlipm and nhips are the lipm and hips techniques but on a Nuclepore substrates. clipm is absorption of coarse particles as measured using the lipm technique on a Teflon substrate.*

Using $b_{ath,2.5\mu m}$ data, Equation (6.10) yields 5.0, 0.8, and 0.5 m^2/g for E1+E2 (EC), O4+OP (high temperature) and pyrolized carbon, and soil, respectively. These absorption efficiencies are more in line with theoretical calculations. For more information on the effect of mixed carbon aerosols, in the form of enclosed chain aggregates, single carbon particles as a function of size and orientation, the reader is encouraged to read a detailed analysis of these considerations by Fuller et al. [1999].

Based on the above derived efficiencies 41%, 34%, and 25% of the absorption is identified with EC, high temperature and pyrolized carbon, and soil, respectively. Across the IMPROVE network, similar apportionments using LIPM yielded 41%, 45%, and 14%. Because the correlation between $b_{ath,2.5\mu m}$ and $b_{abs,2.5\mu m}$ using LIPM are high, the apportionments using either technique are nearly the same.

6.2.6 Reconciliation Between Measured and Scattering Reconstructed From Aerosol Measurements

The theoretical issues concerning reconstructing scattering and extinction from aerosol measurements are discussed in Section 6.1.2. In the most general sense, $b_{scat} \neq \Sigma e_i Mi$, where e_i are species specific mass extinction efficiencies and M_i are the associated species masses [Ouimette and Flagan, 1982]. However, a number of investigators have shown that both on a theoretical [Ouimette and Flagan, 1982] and empirical basis [Malm et al., 2000; Sloane, 1986; Malm, 1998] that the assumption of an externally mixed aerosol and $b_{scat}=\Sigma e_i M_i$ is only 5-10% different from internally mixed assumptions. Therefore, for the Grand Canyon study scattering estimates based on aerosol species measurements are made using:

$$b_{scat,2.5\mu m} = (2.2)([(NH_4)_2 SO_4] + [NH_3 NO_3])\, f(RH) + (4)[OMC] + (1)[SOIL] \qquad (6.11)$$

where $b_{scat,2.5\mu m}$ is scattering associated with particles less than 2.5 μm and enclosed in the brackets are aerosol species mass concentrations. The parenthetically enclosed numerals in front of OMC and SOIL are the optimal dry mass scattering efficiencies as reviewed by White [1990] and Malm et al. [1994]. Furthermore, a nominal mass scattering efficiency value of 3.0 m^2/g was recommended for ammonium sulfate, however, more recent mass size distribution measurements of sulfate suggest a value of about 2.2 m^2/g for the Grand Canyon region [Malm and Pitchford, 1997]. The ratio between dry and wet scattering as a function of RH is the relative humidity scattering enhancement factor, *f*(RH).

For the purposes of the calculations presented here, *f*(RH) was calculated on the basis of Tang's [1996] curves for ammonium sulfate but smoothed between the deliquescent and crystallization branches. Based on size distributions of sulfate at Grand Canyon National Park [Malm and Pitchford, 1997], the assumed geometric mass mean diameter (d_g) was 0.2 μm, while the geometric standard deviation (σ_g) was 2.3. Summary statistics for the *f*(RH) factor, measured and reconstructed PM2.5 scattering as well as scattering associated with each species assuming nominal dry scattering efficiencies and an external mixture are shown in Table 6.11.

Table 6.11 *Statistical summary of measured $b_{scat,2.5\mu m}$, reconstructed scattering, as well as the scattering associated with each aerosol species assuming an external mixture. OCHM refers to organics derived from hydrogen.*

Variable	Mean (1/Mm)	Std. Dev. (1/Mm)	Minimum (1/Mm)	Maximum (1/Mm)	Valid
$b_{scat,2.5\mu m}$	7.03	3.54	1.94	15.50	36
Reconstructed	10.39	4.01	4.91	19.71	36
$(NH_4)_2SO_4$	3.45	2.64	0.76	11.52	36
NH_4NO_3	0.49	0.32	0.10	1.35	36
OCHM	5.82 (2.62)	1.82 (0.82)	3.38 (1.52)	10.08 (4.52)	36
$Soil_{scat}$	0.63	0.26	0.25	1.28	36
f(RH)	1.40	0.58	1.00	4.13	36

The use of nominal scattering efficiencies have, for the most part, worked well for developing estimates of scattering from measured aerosol species concentrations [Malm et al., 1994, 2000; Trijonis et al., 1990]. However, Figure 6.21, a scatter plot of reconstructed and measured scattering, along with the 1:1 line, for the Grand Canyon data set shows poor agreement between these two variables. The estimated or reconstructed scattering is, on the average, overestimated by 3.36 1/Mm or about 50% of measured fine particle scattering.

The choice of nominal scattering efficiencies presented in Equation (6.11) can be explored using multiple linear regression analysis first proposed by White and Roberts [1977] and used by many other authors [Trijonis et al., 1990]. The use of the f(RH) term linearizes the otherwise nonlinear response of hygroscopic aerosol scattering to ambient relative humidity. The results of the regression are presented in Table 6.12. The dependent variable is $b_{scat,2.5\mu m}$, while $[(NH_4)_2SO_4] + [NH_4NO_3]$, organics, and soil are the independent variables. If the choice of nominal scattering coefficients are consistent with measured scattering and the variables are not excessively collinear with each other, then the regression coefficients would equal one.

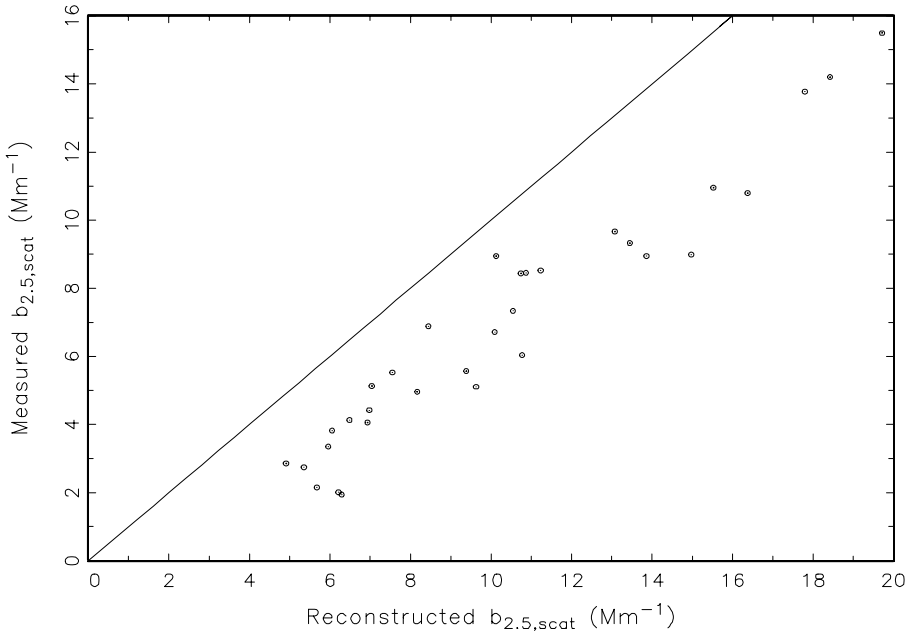

Figure 6.21 *Scatter plot of measured and reconstructed fine particle scattering along with the 1:1 line when nominal values of mass scattering efficiencies were used.*

The coefficient of determination (R^2) is high at 0.91 and the standard errors are small for sulfates (±6%) and organics (±16%), while the regression coefficient associated with soil is not significant. The regression results imply that the assumed dry mass scattering efficiency estimates for sulfates was about right at 2.2 m^2/g, while organics are high by about 65%. Figure 6.22 is the same data as shown in Figure 6.21 but with the organic mass scattering efficiency reduced to 1.8 m^2/g instead of the nominal value of 4.0. The data points are scattered about the 1:1 line and the overall R^2 is near 0.91. Table 6.11 also shows the scattering estimates for organics with the reduced scattering efficiencies parenthetically.

Table 6.12 *Summary table of an ordinary least square regression with $b_{scat,2.5\mu m}$ as the dependent variable and estimates of scattering by sulfate + nitrate, organic by hydrogen, and soil as the independent variables.*

Valid cases: 36	Dependent variable: $b_{scat,2.5\mu m}$			R^2=0.91	
Variable	Estimate	Std error	t-value	Prob t>|t|	Cor dep var
$(NH_4)_2SO_4$+NH_4NO_3	1.01	0.06	17.78	0.000	0.97
OCHM	0.45	0.07	6.17	0.000	0.94
Soil	0.79	0.48	1.64	0.11	0.83

Figure 6.22 *Scatter plot of measured and reconstructed fine particle scattering along with the*

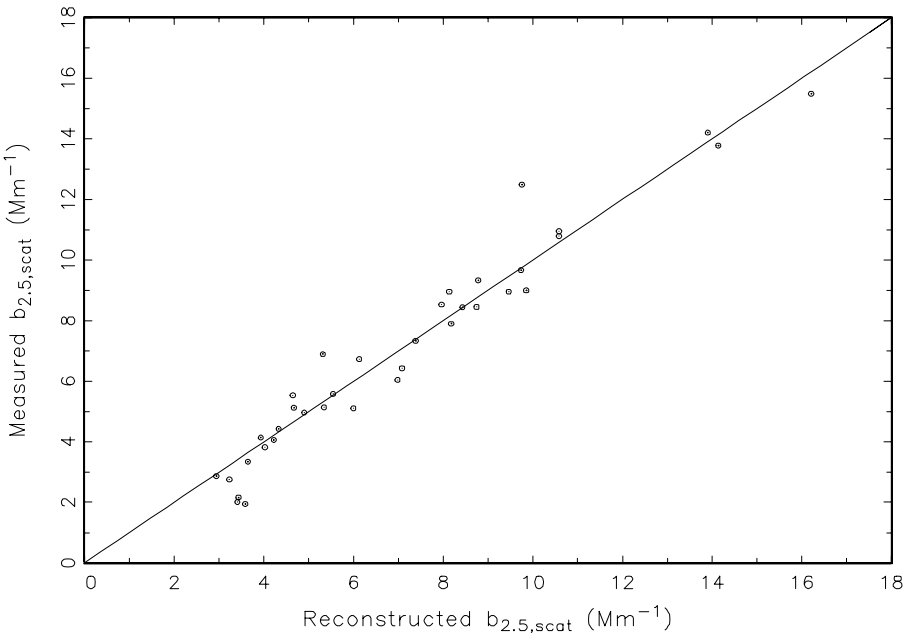

1:1 line when the nominal value of the organic dry mass scattering efficiency was lowered from 4.0 m^2/g to 1.2 m^2/g.

The lower fine organics mass scattering efficiency is consistent with comparatively high coarse mass efficiencies. Only 37% of measured organics are in the fine mode suggesting, assuming something like a lognormal mass size distribution, that the average organic mass mean diameter may be shifted toward the 2.5 μm cutpoint of the cyclone used to separate particles into the "fine" and "coarse" mode.

6.3 HYGROSCOPIC CHARACTERISTICS OF AEROSOLS AT GRAND CANYON AND GREAT SMOKY MOUNTAINS NATIONAL PARKS

The ability of atmospheric particulates to absorb water can be a significant factor in determining its scattering cross section and hence its effect on visibility and/or radiative forcing. For instance, at 90% relative humidity the scattering cross section of typical ammonium sulfate aerosols can be increased by a factor of five or more over that of a dry particle. The hygroscopicity of pure as well as inorganic salts has been studied in the laboratory [Tang, 1996]. It has been well established that inorganic pure salts exhibit deliquescent properties when exposed to moist atmospheres. Moreover, droplet growth can be estimated for both pure and mixed inorganic aerosols purely on the basis of chemical equilibrium equations along with mass concentrations and ion balances [Saxena and Hildemann, 1996; Kim et al., 1994].

On the other hand, organics and their affinity for water, especially those found in the ambient atmosphere, are less well characterized. Organic particulate matter contains hundreds of compounds that cover a wide range of carbon numbers and functional groups Saxena and Hildemann [1996]. They further point out that only a small fraction of potentially nonpolar organics are typically extracted from ambient samples because organic solvents used are typically nonpolar. However, Cadle and Groblicki [1982] and Turpin et al. [1997] have carried out water extractions that would consist of polar organics. Dicarboxylic acids, ketoacids and dicarbonyls have been identified in these extractions although there may be unidentified compounds as well. Typically, less than 10% of the organic matter is identified.

Rather than attempting to identify specific compounds that may be hygroscopic some workers have explicitly measured water uptake of organic material emitted by various source types. For instance, McDow et al. [1994] measured water uptake by diesel soot, automobile exhaust and wood smoke particles. They found that all three emission types absorbed water with wood smoke sample weight increasing by about 10% as sample relative humidity increased from 40-90%. Over the same range of relative humidities, diesel soot sample weight increased by only 2-3%. Chughtai et al. [1999] examined the hydration characteristics of BP2000 (commercially available carbon black), n-hexane, diesel, JP8 (aviation fuel), pine needle, Utah coal, and acetylene. They examined water adsorption isotherms between 20 and 85% relative humidity. They concluded that black carbons produced from a variety of fuel types generally increased with age and surface oxidation and that at high relative humidities (83%) large surface areas determine the adsorption capacity, while at lower humidities the surface functional groups play the most significant role. However, even at 83% relative humidity the water uptake was less than 10% of total mass for all carbon species other than BP2000. Because of its large surface area BP2000 absorbed about 40% of its mass in water. Consequently, they concluded that commercial carbon blacks are not acceptable models for fuel produced carbons.

Other workers have experimentally measured growth of ambient particles as a function of relative humidity [Zhang et al., 1993, 1994; McMurry et al., 1996] using tandem differential mass analyzers (TDMA). One study was carried out at Meadview, Arizona (west end of Grand Canyon) over a 31-day period during the summer of 1991, a second at Hopi Point Arizona (midpoint of Grand Canyon), a 13-day period during winter 1990, while a third was implemented at Claremont, California over an 11-day period during the summer of 1987. A TDMA consists

of two DMAs operated in series. The first DMA is used to select a size, while the second is used to measure the growth of these particles as relative humidity is varied. Usually, a MOUDI size sampler [Marple et al., 1991] is run concurrent with the TDMA to derive estimates of particle composition.

At Grand Canyon, the particles are grouped into three categories: more hygroscopic containing sulfates nitrates and some carbon, less hygroscopic containing carbon mass not accounted for by the number fraction of the more hygroscopic particles, and hydrophopic. Saxena and Hildemann [1996], based on their modeling assumptions, concluded that at Grand Canyon organics add to water absorption by inorganics, while at Claremont the net effect of organics is to diminish water absorption by inorganics. On the other hand, Pitchford and McMurry [1994] were able to show that if one assumed sulfates uptake water at the same rate as measured in the laboratory, they alone could account for all water absorption at Grand Canyon.

Other studies, originally initiated by Covert et al. [1979] examined the scattering characteristics of ambient aerosols as a function of relative humidity. One nephelometer was operated at 30% relative humidity, while a second at variable relative humidity. They made limited measurements $f(RH)=b_{wet}/b_{dry}$ at Tyson, Missouri and Point Reyes, California. The instrumentation was modified and additional measurements of b_{wet}/b_{dry} were made in rural West Virginia and University of Houston, Texas [Waggoner et al., 1983]. Humidity was controlled by first diluting sample air with dry air and then humidifying with a variable amount of water vapor. They also operated a heater and cooler in series with the humidifier (thermidograph), which allowed them to infer compositional structure of the aerosol.

They were able to dry the aerosol to about 30% RH and their first *f(RH)* data points start at about 35%. The singular most interesting feature of their *f(RH)* curves for Shenandoah is that they appear to be continuous over the range of RH values that they measured; that is they did not show evidence of supersaturation. On the other hand, at Houston, Texas, they concluded that the particles were supersaturated about 1/3 of the time. The range of *f(RH)* values at 90% RH varied from a low of about 1.5 to a high of about 2.2- 2.6. Moreover, at Shenandoah, the thermogram measurement allowed them to extract only sulfate scattering at 65-70% RH and it was their conclusion that at 70% RH all the water, within the uncertainty of their measurements, is associated with the ammonium plus sulfate fraction of fine particle mass.

The understanding of the hygroscopic properties of ambient aerosols was in part the motivation for two measurement programs included in this report. The inability to conclusively apportion about 30-50% of the extinction budget between coarse mass scattering and particle absorption at many of our national parks is also seen as important motivating factors.

To address these issues, two studies were carried out, one in the eastern United States at Great Smoky Mountains National Park and the other at Grand Canyon National Park. The design of the Great Smoky study was discussed in Section 6.1, while the Grand Canyon study is presented in Section 6.2. This section will focus on the qualitative and quantitative aspects of measured *f(RH)* curves as a function of aerosol species concentrations. A statistical technique to estimate the aerosol growth of individual species will be presented and results from the two studies compared.

6.3.1 General Features of the $f(RH) = b_{scat}(RH)/b_{scat,Dry}$ Curves

The ratio between dry and wet scattering as a function of RH is referred to as the relative humidity scattering enhancement factor, *f(RH)*. Figure 6.23 shows all the *f(RH)* data points for the Great Smoky data set, while Table 6.13 gives a statistical summary of that data. Over the course of the study, ammonium to sulfate molar ratios varied from a low of 0.30 to a high of 1.85 with an average of 1.1±0.30. A single outstanding feature of the data, although not explicitly observable from the data presentation in Figure 6.23, is the lack of evidence for deliquescence. In spite of the fact that the aerosol was typically dried to about 5-10% the scattering enhancement factor, *f(RH)*, for the most part showed a continuous increase from less than 20%.

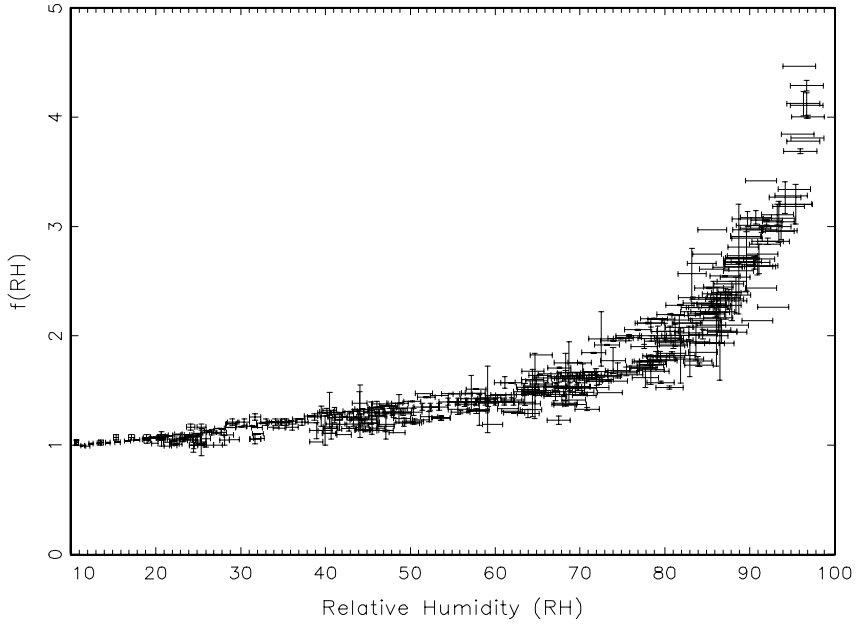

Figure 6.23 *Scatter plot of all measured f(RH) data points collected during the Great Smoky study.*

Figure 6.24, a curve similar to Figure 6.23, shows the *f(RH)* data collected at Grand Canyon. Because of the increased number of data points the average of all *f(RH)* values for a given run and within a given RH range is plotted instead of individual data points. A statistical summary of the data is presented in Table 6.14. As with the Great Smoky data set the *f(RH)* curves did not show evidence of deliquescence in that the curves showed a continuous increase with increasing relative humidity. However, while the Great Smoky data set showed increases in *f(RH)* starting at relative humidity values around 20%, the Grand Canyon data set did not show substantial increases until 40-50%.

Referring to Tables 6.13 and 6.14 the mean *f(RH)* in the 20-25% relative humidity range at Great Smoky was 1.06, while at Grand Canyon it was 1.0; in the 35-40% relative humidity range the *f(RH)* was 1.21, at Great Smoky, while at Grand Canyon it was only 1.05. In the higher relative humidity ranges, the Great Smoky *f(RH)* values always exceeded those of Grand Canyon but by smaller fractional amounts.

Table 6.13 *Statistical summary of mean f(RH) values in selected relative humidity ranges for the Great Smoky data set.*

Relative Humidity	Mean	Std. Dev.	Predicted	Minimum	Maximum	N
20<RH≤25	1.06	0.036	1.01	0.99	1.16	36
25<RH≤30	1.11	0.07	1.04	1.00	1.21	18
30<RH≤35	1.16	0.06	1.06	1.05	1.25	17
35<RH≤40	1.21	0.07	1.09	1.03	1.29	12
40<RH≤45	1.22	0.08	1.14	1.10	1.38	27
45<RH≤50	1.27	0.08	1.20	1.11	1.38	29
50<RH≤55	1.33	0.10	1.27	1.20	1.47	17
55<RH≤60	1.38	0.08	1.35	1.19	1.51	17
60<RH≤65	1.45	0.10	1.45	1.29	1.68	26
65<RH≤70	1.55	0.12	1.58	1.23	1.82	33
70<RH≤75	1.65	0.17	1.73	1.33	1.98	23
75<RH≤80	1.83	0.17	1.91	1.57	2.16	31
80<RH≤85	2.10	0.23	2.12	1.53	2.75	43
85<RH≤90	2.46	0.29	2.43	1.93	3.07	48
RH>90	3.17	0.29	3.01	2.14	4.47	40

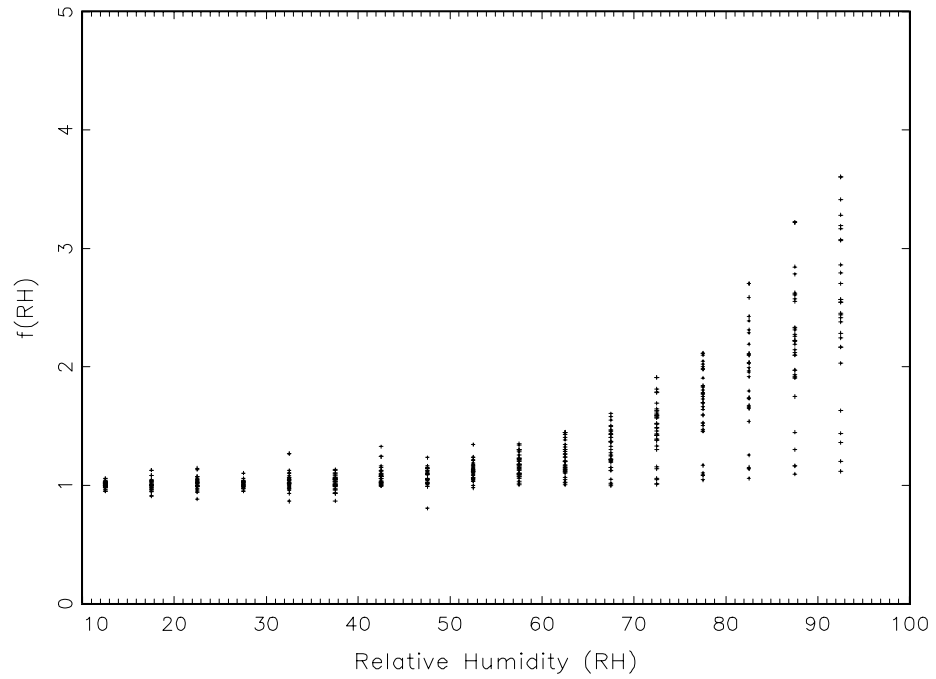

Figure 6.24 *Scatter plot of measured f(RH) data points that have been averaged into 5% relative humidity "bins" for the Grand Canyon data set. The total number of data points for this data set was approximately 7500.*

Table 6.14 *Statistical summary of mean f(RH) values in selected relative humidity ranges for the Grand Canyon data set. Also shown are the corresponding theoretical estimates of f(RH).*

Relative Humidity	Mean	Std. Dev.	Predicted	Minimum	Maximum	N
15≤RH<20	0.99	0.08	1.00	0.68	1.47	350
20≤RH<25	1	0.09	1.00	0.68	1.54	195
25≤RH<30	1.01	0.1	1.00	0.71	1.43	343
30≤RH<35	1.03	0.11	1.00	0.6	1.39	327
35≤RH<40	1.05	0.12	1.01	0.65	1.5	319
40≤RH<45	1.08	0.13	1.06	0.69	2.18	361
45≤RH<50	1.10	0.13	1.11	0.63	1.66	395
50≤RH<55	1.15	0.13	1.17	0.74	1.56	493
55≤RH<60	1.21	0.15	1.24	0.87	1.89	559
60≤RH<65	1.27	0.18	1.33	0.65	1.82	557
65≤RH<70	1.36	0.19	1.43	0.83	1.84	829
70≤RH<75	1.46	0.24	1.55	0.94	2.43	622
75≤RH<80	1.63	0.32	1.70	0.71	3.58	620
80≤RH<85	1.92	0.38	1.87	0.94	4	725
85≤RH<90	2.24	0.48	2.14	1.07	4.84	835

Figure 6.25 shows a "typical" run carried out on Julian day 212. The solid line corresponds to a theoretical prediction of *f(RH)*, which will be discussed in the next section. On this day, 48% and 8% of the fine mass was in the form of sulfates and nitrates, respectively, and significant growth did not occur until about 60% relative humidity. Figure 6.26, another growth curve where sulfates and nitrates made up 39% and 7% of the fine mass, shows an increase in *f(RH)* starting at 45-50% relative humidity rather than at 60%.

Figures 6.25 and 6.26 correspond to hygroscopic inorganic (sulfates and nitrates) fractions of 56% and 46%, respectively, and should be contrasted with Figure 6.27, which shows the *f(RH)* curve on a day when the 24-hr average inorganic hygroscopic fraction was only 22%. Again the solid lines represent theoretical *f(RH)* curves based on measured aerosol concentrations. Julian day 217 was associated with smoke from a forest fire on the north rim of the Grand Canyon. The measured ambient extinction and scattering showed short-term variability throughout the day and therefore the 24-hr aerosol measurement is unlikely to be representative of the time the *f(RH)* curve was measured. In fact, the *f(RH)* curve shown in Figure 6.27 does not show a continuous increase in *f(RH)* over the whole relative humidity range. *f(RH)* increases from 40-57% relative humidity and then is suppressed somewhat with less increase in the 65-80% range.

Figure 6.28 shows a similar plot for the Great Smoky data set. On Julian days 207, 211 and 224 the hygroscopic inorganic fractions were 32.6, 42.7, and 63.5%, respectively. The higher the fraction content of inorganic hygroscopic material the greater the increase in *f(RH)* as a function of relative humidity.

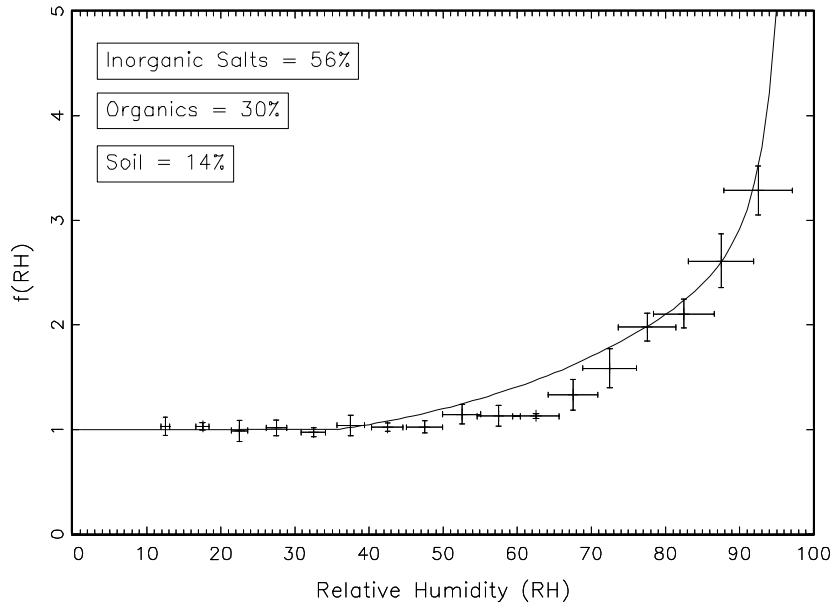

Figure 6.25 *Plot of measured f(RH) on Julian day 212 are presented as data points with uncertainty bars. The uncertainty bars represent a ±5% uncertainty for measured relative humidity, while the uncertainty bars for f(RH) represent one standard deviation of all measurements made within one 5% relative humidity range. The solid line is the result of a theoretical estimate of f(RH). On Julian day 212 the inorganic fraction of fine mass was 56%, organics 30% and soil 14%.*

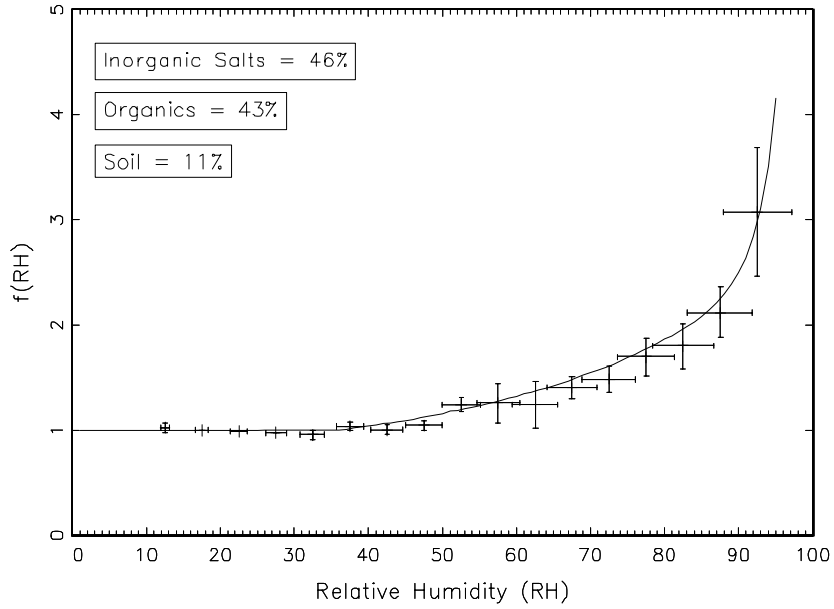

Figure 6.26 *Plot of measured f(RH) on Julian day 204 are presented as data points with uncertainty bars. The uncertainty bars represent a ±5% uncertainty for measured relative humidity, while the uncertainty bars for f(RH) represent one standard deviation of all measurements made within one 5% relative humidity range. The solid line is the result of a theoretical estimate of f(RH). On Julian day 204 the inorganic fraction of fine mass was 46%, organics 43% and soil 9%.*

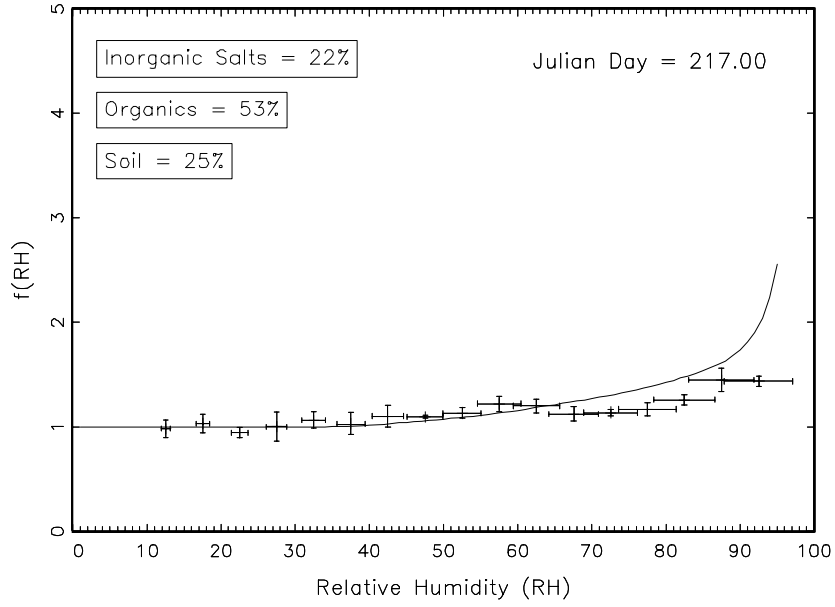

Figure 6.27 *Plot of measured f(RH) on Julian day 217 are presented as data points with uncertainty bars. The uncertainty bars represent a ±5% uncertainty for measured relative humidity, while the uncertainty bars for f(RH) represent one standard deviation of all measurements made within one 5% relative humidity range. The solid line is the result of a theoretical estimate of f(RH). On Julian day 217 the inorganic fraction of fine mass was 22%, organics 53% and soil 25%.*

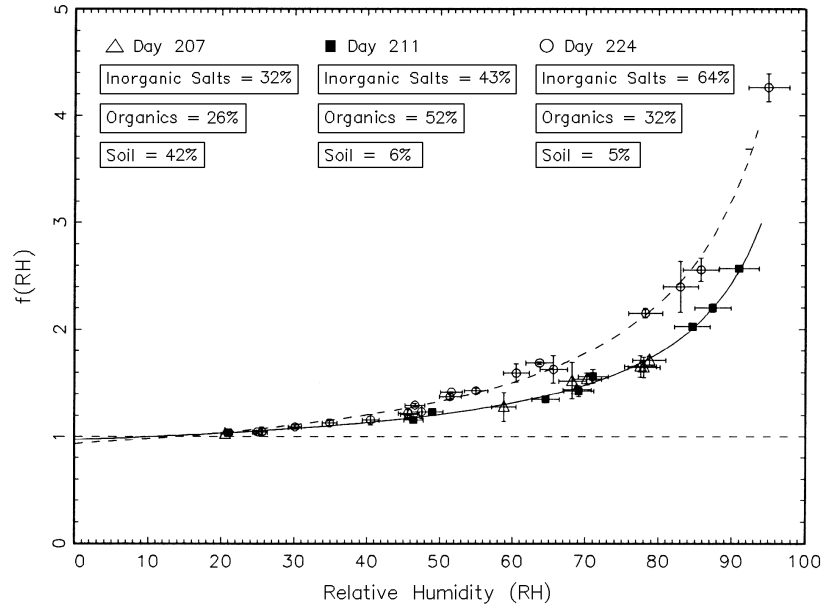

Figure 6.28 *Plot of measured f(RH) on Julian days 207, 211, and 224 for the Great Smoky data set. The uncertainty bars represent a ±5% uncertainty for measured relative humidity, while uncertainty bars on the f(RH) function reflect the instrumental uncertainty associated with the humidograph. The solid line is the result of a theoretical estimate of f(RH). The enclosed captions reflect the relative amounts of inorganic, organic, and crustal material.*

6.3.3 Comparison of Measured *f(RH)* With Theoretical Predictions

Malm et al. [2000] report on a comparison between measured and modeled $b_{scat}(RH)/b_{scat,dry}$ ratios for the Great Smoky data set. Models, described previously, used for the comparison were external with constant mass scattering but with sulfate ammoniation and associated growth accounted for, external with sulfate size, ammoniation, and growth incorporated, and the mixed model. In most cases, all three modeling approaches agreed well with each other, however, the ratios predicted by the internally mixed and external models at times differed from each other under high relative humidity conditions by as much as 30%, with the internally mixed model showing less increase in scattering than the external models.

Measured ratios, in general, were well reproduced by all of the modeling approaches. The R^2 between measured and modeled ratios varied from 0.92 to 0.71, with the external models having the highest R^2. All models, under higher relative humidity conditions, yielded ratios that were on the average greater than those that were measured. The largest discrepancies occurred when organic mass concentrations were highest with modeled ratios being greater than those measured.

For the Grand Canyon study, size distribution data were not available and because little difference is observed between the internally mixed and external models only the external model will be considered here. The following equation is used to estimate scattering under the assumptions of external mixing, constant dry mass scattering efficiencies, and sulfate interpreted as ammonium sulfate:

$$b_{scat} = (2.2)\, f(RH)[SULFATE + NITRATE] + (1.8)\, f_{org}(RH)[OMC] + (1)[SOIL] \qquad (6.12)$$

b_{scat} is the scattering coefficient; [SULFATE] is the SO_4 ion mass concentration adjusted to ammonium sulfate; [NITRATE], [OMC], and [SOIL] are the concentrations of ammonium nitrate, organic carbon, and soil, respectively. The coefficient numbers refer to the assumed dry mass scattering efficiencies of the respective species in units of m^2/g. *f(RH)* and $f_{org}(RH)$ refer to the scattering enhancement factors for sulfates, nitrates, and organics, respectively. The choice of mass scattering efficiencies is discussed in Malm and Day [2000] and is based on recent measurements of sulfur size distributions and on multiple regression analysis of measured $PM_{2.5}$ scattering and aerosol mass concentrations.

The function, *f(RH)*, was calculated on a sampling-period-by-sampling-period basis using Tang's sulfate D/D_o curves. Estimates of *f(RH)* are based on growth curves that were smoothed between the crystallization and deliquescent points. A lognormal sulfate species mass size distribution with a geometric mass mean diameter of 0.2 μm and a geometric standard deviation, σ_g of 2.3 was assumed. The *f(RH)* associated with nitrates was assumed to be the same as for sulfates, while $f_{org}(RH)$ for organics was set equal to one.

As pointed out previously the *f(RH)* curves were continuous showing little evidence for deliquescence. One question we wished to address was the validity of using growth curves that have been smoothed between the deliquescent and crystallization branches. Figures 6.25, 6.26 and 6.27 show the theoretical calculation of the growth curves as solid lines, while the data

points with associated error bars are measured. Figure 6.26 shows a case where measured and predicted estimates compare quite favorably, and the growth curves smoothing assumption appears to reproduce measured data. However, Figure 6.25 shows a case where growth assumptions result in an overprediction of scattering in the 50-75% relative humidity range. There were a number of sampling periods where the estimated *f(RH)* curves were overestimated in this same relative humidity region.

The differences between measured and estimated *f(RH)* values for different relative humidity regions is summarized in Table 6.14. The average of all measured *f(RH)* values within a certain relative humidity range compare favorably to theoretically predicted values, however, the agreement is slightly better at low and high relative humidities than at mid-range humidities. Moreover, under high relative humidity conditions the average measured values are about 2-5% greater than predicted, while around 60% relative humidity the predicted values on the average are about 5% greater. At low relative humidities, measured *f(RH)* shows growth starting as low as 25% RH and increasing slowly to 1.05 at the 35-40% RH range, while the theoretical calculations show zero growth or no change from one in this same range.

An ordinary least square (OLS) regression between measured and predicted *f(RH)* values yields an R^2= 0.82 with slope of 1.02 ±0.006 when the intercept term is forced through zero. The implication is that, on the average, predicted *f(RH)* values are about 2% greater than measured.

Table 6.13 summarizes that same information for the Great Smoky data set for the assumptions of an externally mixed aerosol with corrections for ammoniation and particle size. In the case of the Great Smoky data set, there is some bias in that *f(RH)*, and thereby growth, is underpredicted at lower RH values but overpredicted above about 70% RH. The overall R^2, however, associated with an OLS regression between the two variables is 0.92.

6.3.3.1 Statistical Estimates of $b_{scat}(RH)/b_{scat,dry}$

The amount of scattering at a specific relative humidity can be estimated using:

$$b_{scat,water}(RH) = a_0 + a_1 Sulfate + a_2 Organic + \ldots + a_n Other\ Species \qquad (6.13)$$

where $b_{scat,water}(RH)$ is scattering due to water at some RH, $a_1 = e_s[f(RH)_s+1]$, $a_2=e_{oc}[f(RH)_{oc}+1]$ and so forth. a_o is interpreted as scattering associated with residual water. e_s and e_{oc} are the average dry mass scattering coefficients associated with sulfates and organics, respectively. $b_{scat,water}(RH)=b_{scat}(RH)-b_{scat,dry}$ is calculated on a sampling-period-by-sampling-period basis by estimating $b_{scat}(RH)$ using measured $b_{scat}(RH)/b_{scat,dry}$ ratios and then differencing scattering at some RH and dry scattering. Equation (6.13) can then be solved at specific humidities using OLS regressions with or without an intercept.

For the Great Smoky data set, the coefficients for sulfate are highly significant for all relative humidities for both the intercept and nonintercept models, while the coefficient associated with organics is significant at better than the 5% level for humidities greater than 50% for the zero

intercept model and greater than 25% for the nonzero model. R^2s varied from a low of 0.89 to a high of 0.98.

Figure 6.29 is a plot of the *f(RH)* curves derived from the OLS analysis with an intercept term for sulfates and organics assuming e_s=2.4±0.5 m^2/g and e_{oc}=4.0 m^2/g. The error bars represent the standard error of the regression coefficients, while the rectangle enclosing each error bar is associated with the standard deviation of the theoretically calculated dry scattering coefficients (2.4±0.5 m^2/g) that are based on measured sulfate size distributions. The solid lines are the theoretically calculated *f(RH)* curves for ammonium bisulfate and sulfuric acid assuming D_g=0.36 μm and σ_g = 1.92 [Malm et al., 2000]. The average molar ratio of ammonium to sulfate for the study was near one, however, on the higher sulfate days the molar ratio tended to values less than one, while on lower sulfate concentration days the sulfate aerosols were more neutralized. It is the higher mass concentrations that tend to influence the regression coefficients most and therefore the statistically derived *f(RH)* curve is somewhat greater than the ammonium bisulfate curve but significantly less than the sulfuric acid *f(RH)* curve.

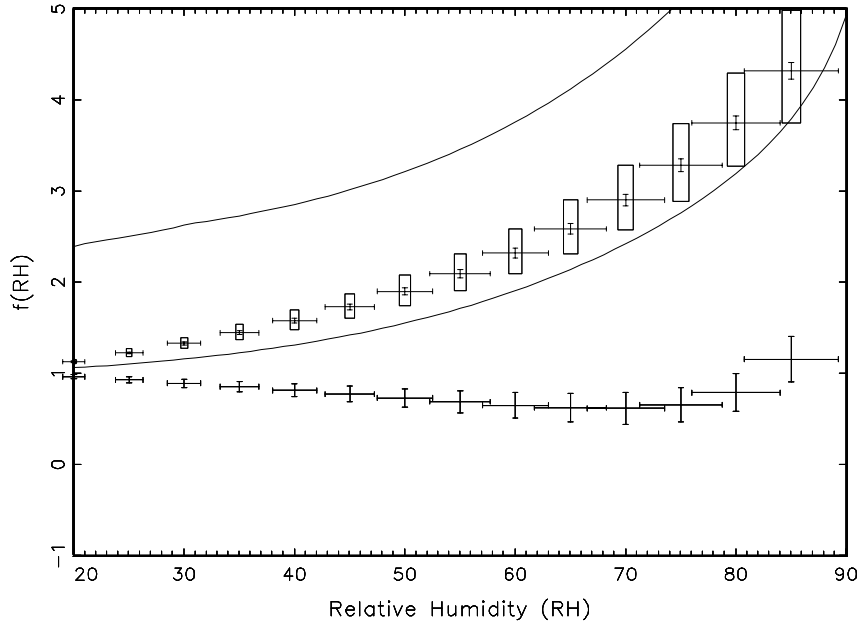

Figure 6.29 *f(RH) is plotted as the solid and broken line for ammonium bisulfate and sulfuric acid, respectively, while the single data points with error bars show the OLS regression with an intercept derived f(RH) for sulfates and organics. The error bars correspond to the standard errors of the regression coefficients, while the upper and lower edges of the rectangle represent the f(RH) that corresponds to ±1 standard deviation of dry mass scattering efficiency that was calculated from measured size distributions.*

An interesting feature of the regressions is the highly significant negative regression coefficients associated with organics. The implication of a negative regression coefficient is reflected in the organic *f(RH)* curves shown in Figure 6.29. An *f(RH)* curve less than one implies that organics would be less efficient at scattering light than predicted by an equation of the type given in Equation (6.14):

$$[OMC] = (1.4)[OC] \quad (6.14)$$

or that the effect of organics is to reduce the ability of sulfates in a sulfate organic mixture to absorb water and thereby reduce the specific scattering efficiency of the mixture. Although the organic *f(RH)* curve is slightly less than one at all relative humidities, *f(RH)*±standard error, for the most part, overlaps one. Therefore any interpretation concerning organic suppression of water absorption should be considered speculative.

The intercept term is identified as residual or unaccounted for water scattering and varies from about 0.6 1/Mm at 20% RH to 2.82 1/Mm at 65% RH. Because dry scattering was measured at about 15% RH and because nitrates were not included in the regression analysis some residual water scattering can be expected. Theoretical estimates of average nitrate scattering vary from about 0.04 1/Mm at 20% RH to 2.0 1/Mm at 85% RH, while the average sulfate scattering at 15% RH is estimated to be 1.8 1/Mm. Therefore, an intercept term on the order of 2-3 1/Mm is consistent with expected residual water scattering.

Figure 6.30 is for the Grand Canyon data set and is similar to Figure 6.29. The sulfate regression coefficient is significant at less than 1% at all humidities greater than 40%, while the regression coefficient associated with all other species are not statistically significant. Moreover, the intercept term is not statistically different from zero. The R^2s varied between 0.6-0.75. As before the error bars represent the standard error of the regression coefficients, while the rectangle enclosing each error bar represents the standard deviation of theoretically calculated dry scattering coefficients that were based on measured sulfate size distributions [Malm and Pitchford, 1997]. Even though the organic regression coefficients were not statistically significant, the implied organic *f(RH)* curve is included for reference. The solid line corresponds to the theoretically derived *f(RH)* curve for ammonium sulfate assuming a D_g=0.3, a σ_g=2.3 and a D/D_o curve that was interpolated between the deliquescent and crystallization branches of the ammonium sulfate hysteresis curve. On the average, the statistically derived *f(RH)* curves agree well with the ammonium sulfate *f(RH)* curve.

6.3.4 Summary of Hygroscopic Characteristics of Aerosols

The understanding of the hygroscopic properties of ambient aerosols as they relate to visibility impairment was in part the motivation for two measurement programs reported on in this report. Two studies, one at Great Smoky Mountains National Park, the other at Grand Canyon National Park, were designed to enhance our understanding of the hygroscopicity of various aerosol types. The Great Smoky study was carried out from July 15, 1995 through August 25, 1995, while the Grand Canyon study was conducted from July 10, 1998 through August 8, 1998 on the south rim of the Grand Canyon. Scattering as a function of relative humidity was measured with a humidograph allowing for estimates of $f(RH) = b_{scat(wet)}/b_{scat(dry)}$, which is used to develop a better understanding of aerosol growth. Modeling scattering as a function of relative humidity serves to both explore the validity of aerosol growth and mixing models and associated assumptions, and provide an estimate of the hygroscopicity of aerosol species other than sulfates and nitrates.

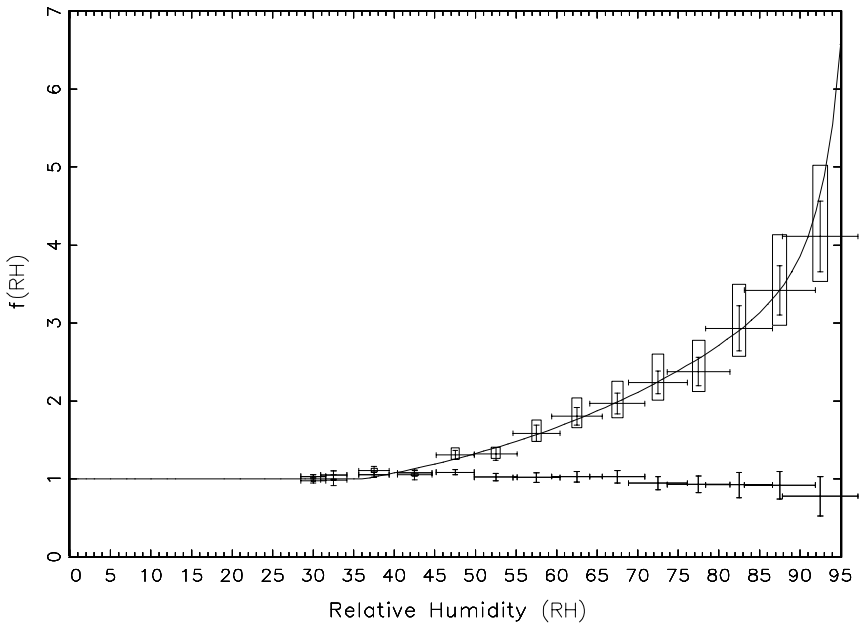

Figure 6.30 *f(RH) is plotted as the solid line for ammonium sulfate, while the single data points with error bars show the OLS regression with an intercept derived f(RH) for sulfates and organics. The error bars correspond to the standard errors of the regression coefficients, while the upper and lower edges of the rectangle represent the f(RH) that corresponds to ±1 standard deviation of dry mass scattering efficiency that was calculated from measured size distributions.*

The *f(RH)* function was smoothly increasing as a function of increasing relative humidity for both data sets. However, for the most part, the *f(RH)* at Great Smoky began to increase at relative humidities of around 20%, while at Grand Canyon increases did not take place until approximately 40-45% and in some cases not until 60%. At Grand Canyon, the *f(RH)* was more varied than at Great Smoky. For instance, in the range of 80-85% relative humidity the *f(RH)* values varied between 1.53 and 2.75 at Great Smoky, while at Grand Canyon the range was from near 1 to 4.0. Part of the explanation of these differences is that in the eastern United States sulfates make up a large fraction of fine mass, while in the West sulfates plus nitrates can actually be a small fraction of fine mass, with organics and soil dust being the major contributors. In general, as organics and soil dust increase the increase of *f(RH)* with humidity decreases.

A variety of scattering models were used to estimate measured *f(RH)* curves. At Great Smoky, an externally mixed aerosol model was assumed with and without sulfate ammoniation, and with and without accounting for sampling-period-to-sampling-period shifts in size distribution. These same variations were explored assuming a mixed aerosol model. The sensitivity to using the deliquescent and crystallization branches as well as a curve smoothed between the deliquescent and crystallization points of D/D_o curves as a function of relative humidity for inorganic salts was also explored. The single most important variables to predicting scattering as a function of relative humidity was accounting for aerosol growth as a function of

sulfate ammoniation and using the smoothed D/D_o growth curves. Changes in *f(RH)* as a function of assumptions concerning mixing were less than 10% on the average.

At Grand Canyon, only the external model was used; sulfate was assumed to be in the form of ammonium sulfate and a smoothed *f(RH)* curve was used based on size distribution measurements made in previous studies. An OLS regression between measured and predicted *f(RH)* values yields a R^2= 0.82 with a slope of 1.02 ±0.006 when the intercept term is forced through zero. The implication being that on the average predicted *f(RH)* values are about 2% greater than measured.

Finally, a model was developed to estimate the *f(RH)* function associated with individual aerosol species. The scattering associated with aerosol water can be shown to relate to aerosol species in a linear way for a given relative humidity. The regression coefficients are functions of dry mass scattering efficiency and $f(RH)= b_{scat}(RH)/b_{scat,dry}$ at a specified relative humidity. The resulting *f(RH)* curve, that is associated with a given data set is interpreted as a weighted average *f(RH)* over the time period corresponding to that data set. At Great Smoky, the measured *f(RH)* was on the average slightly greater than a theoretical curve for ammonium bisulfate implying slightly more growth than would have been predicted from the measured ammoniation (average molar ratio of ammonium to sulfate was one) and size parameters, while at Grand Canyon the measured *f(RH)* curve was nearly identical to the theoretical curve for ammonium sulfate assuming a smoothed D/D_o curve

For both data sets, organics were, within the statistical uncertainty of the regression analysis, judged to be weakly to nonhygroscopic. In fact, for the Great Smoky data set, organics may have repressed the ability of sulfates to absorb water.

6.4 REFERENCES

Air Resource Specialists, Standard operating procedures and technical instructions for nephelometer systems, ARS, 1901 Sharp Point Drive, Ste. E., Ft. Collins, CO 80525, 1994.

Arnott, W.P., Moosmüller, H., Rogers, C.F., Jin, T., and Bruch, R., Photoacoustic spectrometer for measuring light absorption by aerosol: instrument description, *Atmos. Environ.*, **33**, 2845-2852, 1999.

Cadle, S.H. and Groblicki, P.J., An evaluation of methods for the determination of organic and elemental carbon in particulate samples, in G.T. Wolff and R.L. Klimisch (eds.), *Particulate Carbon-Atmospheric Life Cycle*. Plenum Press, New York, pp. 89-109, 1982.

Campbell, D., Perley, B.P., and Eldred, R.A., Measurement of the aerosol absorption coefficient for the IMPROVE Network, *Proceedings Specialty Conference Visual Air Quality: Aerosols and Global Radiation Balance, American Geophysical Union and Air and Waste Management Association*, Pittsburgh, PA, 281-291, 1997.

Chow, J.C., Watson, J.G., Pritchett, L.C., Pierson, W.R., Frazier, C.A., and Purcell, R.G., The DRI thermal/optical reflectance carbon analysis system: Description, evaluation, and applications in U.S. air quality studies, *Atmos. Environ.,* **27A**(8), 1185-1201, 1993.

Chughtai, A.R., Williams, G.R., Atteya, M.M.O., Miller, N.J., and Smith, D.M., Carbonaceous particle hydration, *Atmos. Environ*., **33**, 2679-2687, 1999.

Covert, D.S., Waggoner, A.P., Weiss, R.E., Ahlquist, N.C., and Charlson, R.J., Atmospheric Aerosols, Humidity and Visibility, In *Character and Origins of Smog Aerosols*, John Wiley & Sons, 559-581, 1979.

Day, D.E., Malm, W.C., and Kreidenweis, S.M., Seasonal variations in aerosol composition acidity at Shenandoah and Great Smoky Mountains National Parks, *J. Air & Waste Management Assoc.,* **47**(3), 411-418, 1997.

Dietrich, L., Molenar, J.V., and Faust, J.F., Transmissometer extinction measurements in an urban environment, In *Transactions Visibility and Fine Particles*, (edited by C.V. Mathai), AWMA, Pittsburgh, PA, 374-383, 1989.

Eldred, R.A. and Cahill, T.A., Trends in elemental concentrations of fine particles at remote sites in the United States, *Atmos. Environ.,* **28**(5), 1009-1019, 1994.

Eldred, R.A., Cahill, T.A., Pitchford, M., and Malm, W.C., IMPROVE-A new remote area particulate monitoring system for visibility studies, *Proceedings 81st Annual Meeting of the Air Pollution Control Association*, Pittsburgh, PA, 1988.

Fitzgerald, J.W., Angular truncation error of the integrating nephelometer in the fog droplet size range, *J. Appl. Met*., **16**, 198-204, 1977.

Fuller, K.A., Malm, W.C., and Kreidenweis, S.M., Effects of mixing on extinction by carbonaceous particles, *J. Geophys. Res*., **104**(D13), 15941-15954, 1999.

Gebhart, K. A. and Malm, W. C., An investigation of the size distributions of particulate sulfate concentrations measured during WHITEX, In *Transactions Visibility and Fine Particles*, (edited by C.V. Mathai), AWMA, Pittsburgh, PA, 157-169, 1990.

Hansen, A.D.A., Rosen, H., and Novakov, T., Real-time measurements of the absorption coefficient of aerosol particles, *Appl. Optics*, **21**, 3060, 1982.

Hasan, H. and Lewis, C.W., Integrating nephelometer response corrections for biomodal size distributions, *Aerosol Sci. Technol*. **2**, 443-453, 1983.

Heintzenberg, J. and Quenzel, H., On the effect of the loss of large particles on the determination of scattering coefficients with integrating nephelometers, *Atmos. Environ.,* **7**, 503-507, 1973.

Hitzenberger, R., Jennings, S.G., Larson, S.M., Dillner, A., Cachier, H., Galambos, Z., Rouc, A., and Spain, T.G., Intercomparison of measurement methods for black carbon aerosols, *Atmos. Environ.,* **33**, 2823-2833, 1999.

Horvath, H., Atmospheric light absorption-A review, *Atmos. Environ.,* **27**(A), 293-317, 1993.

Huffman, H.D., Comparison of the light absorption coefficent and carbon measures for remote aerosols: an independent analysis fo data from the IMPROVE network-I, *Atmos. Environ.,* **30**, 73-83, 1996.

John W., Wall, S.M., Ondo, J.L., and Winklmayr W., Modes in the size distributions of atmospheric inorganic aerosol, *Atmos. Environ.,* **24**, 2349-2359, 1990.

Kim, Y.P., Pun, B. K. –L., Chan, C.K, Flagan, R.C., and Seinfeld, J.H., Determination of water activity in ammonium sulfate and sulfuric acid mixtures using levitated single particles, *Aerosol Sci. Tech*., **20**, 275-284, 1994.

Malm, W.C., Examining the relationship between aerosol concentration and partial scattering efficiencies near the Grand Canyon, presented at the *91st Annual Meeting and Exhibition of the Air and Waste Management Association*, Pittsburgh, PA, 1998.

Malm, W.C. and Day, D.E., Optical properties of aerosols at Grand Canyon National Park, accepted for publication in *Atmos. Environ*., 2000.

Malm, W.C. and Kreidenweis, The effects of aerosol hygroscopicity on the apportionment of extinction, *Atmos. Environ.,* **31**, 1965-1976, 1997.

Malm, W.C. and Pitchford, M.L., Comparison of calculated sulfate scattering efficiencies as estimated from size-resolved particle measurements at three national locations, *Atmos. Environ.,* **31**, 1315-1325, 1997.

Malm, W.C., Day, D.E., and Kreidenweis, S.M., Light scattering characteristics of aerosols as a function of relative humidity: Part I-a comparison of measured scattering and aerosol concentrations using the theoretical models, *J. Air and Waste Management Assoc.*, **50**, 2000.

Malm, W.C., Molenar, J.V., Eldred, R.A., and Sisler, J.F., Examining the relationship among atmospheric aerosols and light scattering and extinction in the Grand Canyon area, *J. Geophys. Res.,* **101**, 19251-19265, 1996.

Malm, W.C., Sisler, J.F., Huffman, D., Eldred, R.A., and Cahill, T.A., Spatial and seasonal trends in particle concentration and optical extinction in the United States, *J. Geophys. Res.* **99**, 1347-1370, 1994.

Marple, V.A., Rubow, K.L., and Behm, S.M., A microorifice uniform deposit impactor (MOUDI): description, calibration, and use, *Aerosol Sci. Technol*., **14**, 434, 1991.

McDade, C.E. and Tombach, I.H., Goals and initial findings from SCENES, In *Transactions Visibility Protection, Research and Policy Aspects,* (edited by Bhardwaja, P.S.) APCA, Pittsburgh, PA, 1987.

McDow, S.R., Vartianen, M., Sun, Q., Hong, Y., Yao, Y., and Kamens, R.M., Combustion aerosol water content and its effect on polycyclic aromatic hydrocarbon reactivity, Atmos. Environ., **29**, 791-797, 1994.

McMurry, P.H., Zhang, X., and Lee, C.-T., Issues in aerosol measurement for optics assessment, *J. Geophys. Res*., **101**, 19189-19197, 1996.

Meng, Z., Seinfeld, J.H., and Saxena, P., Gas/aerosol distribution of formic and acetic acids, *Aerosol Sci. Technol.*, **23**, 561-578, 1995.

Molenar, J.V., Analysis of the real world performance of the Optec NGN-2 ambient nephelometer, *Proceedings of Visual Air Quality, Aerosols, and Global Radiation Balance,* AWMA, Pittsburgh, PA., 243-265, 1997.

Molenar, J.V., Dietrich, D.L., and Tree, R.M., Application of a long range transmissometer to measure the ambient atmospheric extinction coefficient in remote pristine environments, In *Transactions Visibility and Fine Particles*, (edited by C.V. Mathai), AWMA, Pittsburgh, PA., 1989.

Moosmüller, H., Personal communication, 1998.

Ouimette, J.R. and Flagan, R.C., The extinction coefficient of multicomponent aerosols, *Atmos. Environ.*, **16**, 2405-2419, 1982.

Pilinis, C., Pandis, S. M., and Seinfeld, J. H., Sensitivity of direct climate forcing by atmospheric aerosols to aerosol size and composition, *J. Geophys. Res.*, **100**, 18739-18754, 1995.

Pitchford, M. L. and McMurry, P. H., Relationship between measured water vapor growth and chemistry of atmospheric aerosol for Grand Canyon, Arizona, in winter 1990, *Atmos. Environ*., 28, 827-839, 1994.

Rotronic Instrument Corp. Humidity-temperature meteorological pro, MP-100F, Fact Sheet, Rotronic Instrument Corp, 160 E. Main Street, Huntingdon, NY 11743, 1998.

Sandberg, D.V., Pierovich, J.M., Fox, D.G., and Ross, E.W., Effects of Fire on Air, General Technical Report WO-9, U.S. Department of Agriculture, U.S. Forest Service, Washington, D.C., 1979.

Saxena, P. and Hildemann, L.M., Water-soluble organics in atmospheric particles: a critical review of the literature and application of thermodynamics to identify candidate compounds, *J. Atmos. Chemistry*, **24**, 57-109, 1996.

Saxena, P. and Peterson, T.W., Thermodynamics of multicomponent electrolytic aerosols, *J. Colloid Interface Sci.*, **79**, 496-510, 1981.

Saxena, P., Hudischewskyj, A.B., Seigneur, C., and Seinfeld, J.H., A comparative study of equilibrium approaches tot he chemical characterization of secondary aerosols, *Atmos. Environ.,* **20**, 1471-1483, 1986.

Saxena, P., Mueller, P.K., Kim, Y.P., Seinfeld, J.H., and Koutrakis, P., Coupling thermodynamic theory with measurements to characterize acidity of atmospheric particles, *Aerosol Sci. Technol.*, **19**, 279-293, 1993.

Saxena P., Hildemann L. M., McMurry P. H., and Seinfeld, J. H., Organics alter hygroscopic behavior of atmospheric particles, *J. Geophys. Res.* **100**, 18755-18770, 1995.

Sisler, J. F., *Spatial and Seasonal Patterns and Long Term Variability of the Composition of the Haze in the United States: An Analysis of Data from the IMPROVE Network,* Cooperative Institute for Research in the Atmosphere, Colorado State University, ISSN 0737-5352-32, 1996.

Sisler, J. F., Huffman, D., Latimer, D. A., Malm, W. C. and Pitchford, M. L., *Spatial and Temporal Patterns and the Chemical Composition of the Haze in the United States: An Analysis of Data from the IMPROVE Network 1988-1991,* Cooperative Institute for Research in the Atmosphere, Colorado State University, ISSN 0737-5352-26, 1993.

Sloane, C.S., Optical properties of aerosols—comparison of measurement with model calculations, *Atmos. Environ.*, **17**, 409-416, 1983.

Sloane, C.S., Optical properties of aerosols of mixed composition, *Atmos. Environ.*, **18**, 871-878, 1984.

Sloane, C.S., Effect of composition on aerosol light scattering efficiencies, A*tmos. Environ.*, **20**(5), 1025-1037, 1986.

Sloane, C.S., Rood, M.J., and Rogers, F.C., Reconciliation of aerosol particle size measurements, In *Transactions Visibility and Fine Particles,* (edited by Mathai C.V.), AWMA, Pittsburgh, PA., 1990.

Stelson A.W. and Seinfeld J.H., Relative humidity and temperature dependence of the ammonium nitrate dissociation constant, *Atmos. Environ.*, **15**, 983, 1982.

Tang, I. N., Chemical and size effects of hygroscopic aerosols on light scattering coefficients, *J. of Geo. Research*, **101**, 19245-19250, 1996.

Trijonis, J.C., RESOLVE project final report, Visibility conditions and causes of visibility degradation in the Mojave Desert of California, NWC Tech. Pap. 6869, Naval Weapons Center, China Lake, CA., 1988.

Trijonis, J.C. and Pitchford, M., *Preliminary extinction budget results from the RESOLVE program*, edited by P.S. Bhardwaja, Visibility Protection Research and Policy Aspects, Air Pollution Control Association, Pittsburgh, PA., 1987.

Trijonis, J.C., Malm, W.C., Pitchford, M., White, W.H., Charlson, R., and Husar, R., Visibility: Existing and historical conditions - Causes and effects. In *State Sci. State Technol. Rep. 24, Natl. Acid Precip. Assessment Program*, Washington, D.C., 1990

Turpin, B.J., Saxena, P., Allen, G., Koutrakis, P., McMurry, P., and Hildemann, L., Characterization of the southwestern desert aerosol, Meadview, Arizona, *J. Air and Waste Management Assoc.*, **47**, 344-356, 1997.

Twomey, S., Comparison of constrained linear inversion and an iterative non-linear algorithm applied to the indirect estimation of particle size distributions, *J. Comput. Phys*. **18**, 188-200, 1975.

Waggoner, A.P., Weiss, R.E., Ahlquist, N.C., Covert, D.S., Will, S., and Charlson, R.J., Optical characteristics of atmospheric aerosols, *Atmos. Environ.,* **15**, 1891-1909, 1981.

Waggoner, A. P., Weiss, R. E., and Larson, T. V., In-situ rapid response measurement of $H_2SO_4/(NH_4)_2SO_4$ aerosols in urban Houston: a comparison with rural Virginia, *Atmos. Environ.,* **17**, 1723-1731, 1983.

Wexler A. and Seinfeld J., Second-generation inorganic aerosol model, *Atmos. Environ.,* **25A**(12), 2731, 1991.

White, W. H., On the theoretical and empirical basis for apportioning extinction by aerosols: a critical review, *Atmos. Environ.,* **20**, 1659-1672, 1986.

White, W.H., Contributions to light scattering, In *Acidic Deposition: State of Science and Technology, Tech. Rep. 24*, pp. 85-102, Natl. Acid Precip. Assess. Program, Washington, D.C., 1990

White, W.H. and Macias, E.A., Light scattering by haze and dust at Spirit Mountain, Nevada, In *Transactions Visibility and Fine Particles*, (edited by C. V. Mathai), AWMA, Pittsburgh, PA., 1990.

White, W.H. and Roberts, P.T., On the nature and origins of visibility-reducing aerosols in the Los Angeles Air Basin, *Atmos. Environ.*, **11**, 803-812, 1977.

White, W.H., Macias, E.S., Nininger, R.C., and Schorran, D., Size-resolved measurements of light scattering by ambient particles in the southwestern U.S.A., *Atmos. Environ.*, **28**, 909-921, 1994.

Zhang, X.Q., McMurry, P.H., Hering, S.V., and Casuccio, G.S., Mixing characteristics and water content of submicron aerosols measured in Los Angeles and at the Grand Canyon, *Atmos. Environ*., **27**A, 1593-1607, 1993.

Zhang, X.Q., Turpin, B.J., McMurry, P.H.,Hering, and S.V.,Stolenberg, M.R., Mie theory evaluation of species contributions to 1990 wintertime visibility reduction in the Grand Canyon, *J. Air Waste Management Assoc.*, **44**, 153-162, 1994.